Sensing fluid pressure during plucking events in a natural bedrock channel: Cowpasture River, VA

B.S. HONORS THESIS IN GEOLOGY

CLARE ELIZABETH WILKINSON

April 2017

Washington and Lee University
Advisor: Dr David Harbor

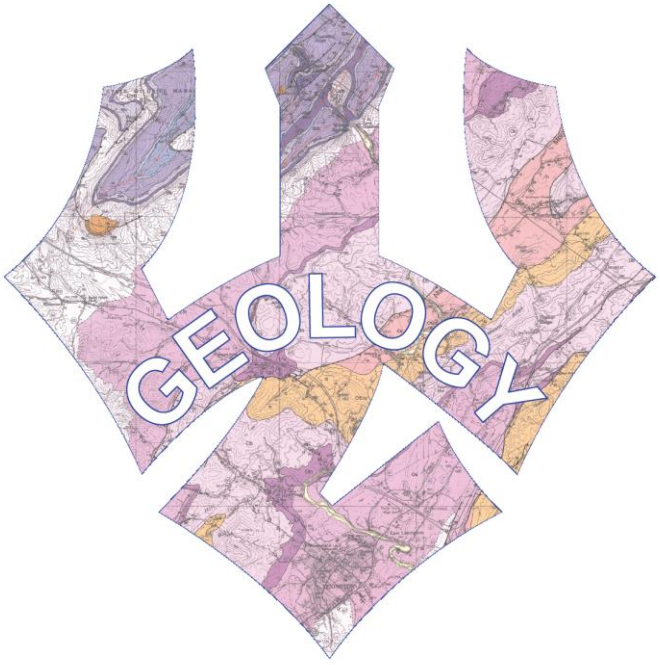

Table of Contents

Abstract

Bedrock river erosion by plucking—the wholesale removal of bedrock blocks—is likely the dominant non-glacial driver of incision into topography over both short- and long-term timescales. Engineering and physical/numerical modeling inform most of our understanding of plucking because the process is difficult and often dangerous to observe and measure in natural channels. Model studies detail controls on the plucking process, including block size, protrusion factor and head change due to hydraulic structures. Engineering studies detail pressure pulse transmission through the joint network of concrete blocks from impinging jets. Natural channels with jointed or fractured bedrock likely also experience a transmission of pressure through the crack network.

Instrumentation of a natural bedrock block is designed to test plucking caused by fluid pressure propagation through the sub-block and crack network. Herein I outline the procedure of designing and constructing a waterproof housing for a suite of electronics that record fluid pressure and movement of a natural bedrock block. To investigate pressure transmission through the sub-block network, I drilled a hole through a bedrock block and installed two MS5308 fluid pressure sensors flush with the top and bottom of a bedrock block. I installed an MPU6050 accelerometer/gyroscope to understand block movement associated with pressure fluctuations. The sensors record data at 40 samples/sec with great sensitivity.

The study site on the Cowpasture River in Bath County, VA is characterized by 5 bedrock steps, each of which produce a hydraulic jump and train of standing waves. An estimated discharge of ~6230 cfs is a minimum for plucking to occur; this discharge was not achieved during the test period but is achievable in a 2- to 5-year flood event.

Acknowledgements

I extend my eternal gratitude to Dr David Harbor, without whom this project would have seen neither conception nor execution. His guidance and support was instrumental throughout the entirety of the project. I am honored to have him as a mentor but even more honored to have him as a friend.

I would also like to thank the Plecker family, who generously allowed me to conduct my study in their beautiful stretch of the Cowpasture River (sorry we didn't find any gold!). Thanks to Dr Simon Levy, whose wizardry in computer science and electronic engineering was invaluable to the implementation of this project. Dr Levy also detailed the methodology for device programming used in this thesis. Thanks to Dr Joel Kuehner for his knowledge and guidance in the realm of fluid dynamics, to Dave Pfaff and Dr Paul Low of the Washington and Lee University IQ center for helping me with 3D printing, to Emily Falls for knowing the answer to every question I asked about the whereabouts of various tools, to Edward Mallon of the Cave Pearl Project, who provided initial inspiration and guidance for our DIY underwater housing for electronics, and to Tal Keel '18, Kyle Turpin '17 and Eleni Timas '17 for their assistance in the field. I would like to thank the entirety of the Washington and Lee Geology department faculty and Sarah Wilson for believing in me and encouraging me to follow my heart and chase my dreams. A big thank you to Elliott Helgans '16, who was a wonderful lab partner during my first summer studying the plucking problem, and to all members of Team Plucking past: Elizabeth Elium '15, James Biemiller '15, James Freeman '16, Jack Wilbur '16 and Murtaza Kapasi '16.

Lastly, I would like to extend a special thanks to the Washington and Lee University Summer Research Scholar program for funding two years of summer research, to the R. Preston Hawkins IV Geology Award for supplemental funding during both summers, and to the Samuel J. Kozak-Odell S. McGuire-Edgar W. Spencer-Frederick L. Schwab Award for supporting my travels to multiple professional conferences to present this research.

1. Introduction

Bedrock channels play a strong role in landscape evolution over geologic time; they are the dominant non-glacial source of incision into topographic relief (Hancock et al., 1998; Whipple et al., 2000a). There is a delicate relationship between erosion and tectonics in which both processes influence the other (Willett, 1999; Whipple, 2004; Lamb et al., 2015). In tectonically active areas, incision by bedrock channels can steepen hillsides and undercut slope toes, which leads to mass removal and material transport from those hillslopes (Whipple et al., 2000b; Hancock et al., 1998). Rivers are a crucial driver of dynamic topography; removal of mass from mountainsides creates a flexural isostatic response that stimulates uplift (Whipple, 2004; Hancock et al., 1998). Tectonism in turn deforms bedrock; in bedrock river channels, the result of such deformation is a joint or crack network across homogenous units (Fig. 1) (Molnar et al., 2007). Though it is accepted that rivers play an integral role in landscape evolution over geologic time, many questions about the exact system dynamics remain; scientists still debate the best way to quantify, characterize and understand bedrock river erosional processes (Tinkler and Wohl, 1998; Wende, 1999; Snyder et al., 2003; Lamb et al., 2015).

Erosion of bedrock in channels occurs by three mechanisms: cavitation, abrasion and plucking (Hancock et al., 1998; Wende, 1999). Cavitation is a process in which entrained bubbles impact the bed and cause microerosion (Tinkler and Wohl, 1998). Cavitation is best understood from an engineering application; the process has been well-documented in studies of dam-spillway and metal turbine erosion but remains largely absent from pure geologic research due to lack of field evidence for the process (Whipple et al., 2000a). Cavitation is, however, posited as a strong candidate for development of potholes (Barnes, 1956; Tinkler and Wohl, 1998; Beer et al., 2015). Erosional potential is enhanced when cavitation works in concert with abrasion (Whipple et al., 2000a). As cobbles and other coarse sediment impact the bed, divots populate the bedrock. These surface irregularities stimulate formation of air bubbles in the flow, promoting cavitation as an erosional mechanism (Sklar and Dietrich, 2004). The challenge in distinguishing between erosional features caused by abrasion and those caused by cavitation—there are no erosional signatures exclusive to cavitation—is what makes confirming cavitation a strong, independent erosional mechanism so challenging (Whipple et al., 2000a).

Abrasion occurs when bedload or entrained sediment impact the bed and act to either smooth or fracture the bed (Hancock et al., 1998). Sediment exerts a frictional force on exposed

bedrock, and finer-grained material essentially sand-blasts the bed to create smooth, rounded, sculpted features (Chatanantavet and Parker, 2009; Freeman, 2016). Larger clasts can fracture or crack flakes of rock away from the bed (Hancock et al., 1998). Effectiveness of abrasion is dependent on kinetic energy of the impacting grains and "erodibility" or susceptibility of the bedrock substrate to abrasion (Hancock et al., 1998; Whipple et al., 2000a; Freeman, 2016). Large clasts, which typically exert the greatest impact force on the bed, contribute to generation and propagation of crack networks (Whipple et al., 2000a). In situations where joint networks are weakly developed, impact by abrading sediment may be key in preparing bedrock for further erosion by plucking (Whipple et al., 2000a).

Plucking is the wholesale removal of river rock blocks solely by flow and is posited as the most effective erosional process in bedrock channels over both short- and long-term geologic timescales (Hancock et al., 1998; Li et al., 2016; Elium, 2015). Moreover, in river reaches where incision is rapid and bedding spacing or jointing is present, plucking is likely the chief erosional mechanism (Hancock et al., 1998; Wende, 1999; Whipple et al., 2000a; Pan et al., 2014; Wilkinson et al., 2015). Plucking in natural settings has been found most effective when the bedrock is "pre-conditioned" (having a pre-existing crack or joint network) and especially when either bedrock joint spacing is 0.1-1 m or broken into blocks with a small height-to-length ratio (Hancock et al., 1998; Whipple et al., 2000a; Snyder et al., 2003). In order for plucking to occur, a rock block must be totally isolated from the surrounding bed (Li et al., 2016). Block isolation occurs through joint expansion, wherein processes such as sediment or debris wedging can drive the cracks apart (Snyder et al., 2003). Cavitation and abrasion may be influential to initiating or developing a crack network, but it is plucking of blocks after the crack network is established that ultimately does the most work in a bedrock channel.

To date, plucking is best understood through engineering case studies and physical or numerical modeling investigations. Pioneering research of plucking revealed that fluid forces can pluck blocks via sliding, rotating or lifting (Figs. 2-3) (Hancock et al., 1998; Wende, 1999; Whipple et al., 2000a). Modeling studies by Coleman et al. (2003)—and later used by Lamb et al. (2015) to develop plucking theory—suggest that plucking only occurs when there is an element of block protrusion. To understand water retreat in basalt on Earth and Mars, Lamb and Dietrich (2009) model erosion of blocks in waterfalls and quantify sliding or toppling of material. Most engineering studies examine scour at the base of plunge pools or jets (Annandale,

2005; Federspiel et al., 2011; Federspiel, 2011; George et al., 2015). Fiorotto and Rinaldo (1992) investigate controls on concrete slab uplift in highly erosive flows in dam spillways. They suggest that size and shape of a bedrock block is an important factor in determining the "pluckability" of a block. Wilkinson et al. (2015) found that plucking of model bedrock occurs in myriad ways and without protrusion.

Though not all researchers investigating the plucking process believe that findings from engineering studies are applicable to natural channels (Coleman et al., 2003), understanding plucking in both artificial and natural channels will inform the engineering and geological communities and foster a deeper understanding of this phenomenon.

1.1 Laboratory flume studies

Laboratory flume studies over the past decade have corroborated and expanded upon early findings by Hancock et al. (1998) and Wende (1999). Dubinski and Wohl (2012) investigated the evolution of a model knickpoint. One of their most profound findings was that sidewall friction between blocks is important for plucking by sliding. Blocks in the center of the flow are more likely to slide out of place than those on the edges of the flume, attributed to drag forces induced by the flume walls on the flow that reduce velocity and render plucking more difficult. Dubinski and Wohl (2012) documented a reduction in sidewall friction over time as blocks undergo in situ weathering. Wilkinson et al. (2015) also found that model bedrock blocks undergo in-situ erosion that enlarges cracks throughout the bed and increases "joint spacing". Their flume studies not only observed plucking by sliding, rotating and lifting, but revealed complex variations of block movement patterns. Tiles of Plaster of Paris model bedrock subjected to all three flow regimes—subcritical, critical and supercritical—moved by lateral, downstream or upstream sliding; rotation or flip; and lift (Figs. 4-5) (Wilkinson et al., 2015).

Wilkinson et al. (2015) propose that plucking occurs due to a dynamic pressure gradient throughout the bed. They suggest that the change in head from the trough to crest of a hydraulic structure—such as a hydraulic jump or standing wave (Fig. 6)—changes bedrock pore pressure, and that model bedrock blocks respond to transmission of high pressure in the sub-block network. They also found that plucking occurs in absence of block protrusion. This finding challenges claims by Coleman et al. (2003) and Lamb et al. (2015) that some degree of protrusion is required for plucking to occur. In an experiment involving multiple layers of model

bedrock, Wilkinson et al. (2015) determined that a hydrostatic head change with a static head 4 times greater than the submerged normal pressure of the model bedrock was sufficient to drive uplift. This equates to a ~8-10 cm-deep model flow with standing waves with a 1-2 cm height difference between crest and trough.

Fluid pressure transmission has been modeled physically by Federspiel et al. (n.d.) and numerically by Li et al. (2016). In the former, pressure fluctuations in spillway plunge pools with impinging jets are augmented within model joint networks and transient fluid pressure oscillations are propagated throughout the cracks. In the latter, fluid pressure fluctuations result in "accumulative plucking" as the block is slowly jacked from the bed.

Plucking in response to fluid pressure transmission and dynamics inspired this project. Given results of model studies, the aim of this study is to quantify pressure fluctuations in both the flow and sub-bed crack network of natural channels and to correlate changes of pressure head to block movement to better understand the relationship between fluid forces and block uplift. Implementation of this study therefore requires instrumenting a "pluckable" bedrock block.

1.2 Advances in monitoring channel sediment

A field of research that has seen an explosion of work over the past few years is sediment tracking. Monitoring sediment movement originated with a study using radio-frequency identification (RFID) to track pebble movement on artificial beaches (Benelli et al., 2009). The authors used RFID tags to capture the movement of sediment to better characterize, visualize and quantify coastal erosion (Benelli et al., 2009). Since then, other studies have used technologically-equipped stones or pebbles to understand trajectories of sediment along shorelines (Bertoni et al., 2012), boulder movement along rocky shorelines (Stephenson and Abazović, 2016), pebbles in scour/plunge pools (Chen et al., 2015), and pebbles in artificial laboratory channels (Gronz et al., 2016).

In most cases, the electronics used to create these "Smartstones" (© Gronz et al., 2016) or "Smart rocks" (© Chen et al., 2015) include sensors that record "orientation, tilt, motion, acceleration, rotation, shock, vibration and heading" (Gronz et al., 2016). George et al. (2015) conducted flume experiments that involved subjecting study blocks to different flow rates. Their experiments involved increasing flume discharge every 5 minutes until the blocks failed. Studies

involving instrumented sediment have in common the use of triaxial accelerometers and gyroscopes, magnets, RFID tags and batteries.

A challenge for conducting studies using electronically-instrumented blocks is waterproofing. Methods for waterproofing used in previous studies include acrylic balls (Chen et al., 2015); mounting a probe inside a real pebble, sealed with waterproof modelling mass (Gronz et al., 2016); and a waterproof plastic container, sealed with four screws and a flat rubber washer (Stephenson and Abazović, 2016).

I intended to design and construct a waterproof capsule that could hold electronic sensors to monitor block movement as well as fluid pressure fluctuations above and below a "pluckable" bedrock block. Before doing so, I had to find a block suitable for instrumentation. I searched for a study site similar to the flume setup from Wilkinson et al. (2015), and identified the Cowpasture River in Bath County, VA as the ideal locality.

1.3 Study site

The study site is a roughly 120-m-long reach along the Cowpasture River in Bath County, VA, located at UTM 4211100N, 617200E (Fig. 7). The Cowpasture River is an 84-mile-long tributary to the James River and has a total drainage area of 461 square miles in Virginia (Elium, 2015). The closest gauge to the study site is downstream in Clifton Forge, VA. The river experiences a number of high water stages annually, which will provide the opportunity to characterize block movement in various types of flow conditions (Fig. 8).

At the study site, the river flows over a series of five distinct, resistant sandstone bedrock steps of the Brallier Formation (USGS Mineral Resources). The hydraulic structures generated by the middle of the five bedrock steps, step 3, mimic those from flume experiments by Wilkinson et al. (2015). Step 3 is 0.9-m-tall, and downstream is the study bed, an 11-cm-thick, medium to dark gray, fine to very-fine grained arkosic quartz sandstone (Fig. 9). Strike is nearly perpendicular to flow and the beds dip only a few degrees upstream. Vertical fractures throughout the bed are linear and nearly parallel to river flow direction. Blocks of bedrock that have slid downstream are evidence that plucking occurs at the study site (Fig. 10). Oddly, unconsolidated sediment ranging in size from silt to cobbles exists under the bed, likely having replaced an eroded layer of weak shale. This sediment is present meters upstream from the

downstream lip of the bed, suggesting that flow drives sediment upstream under the bed (Figs. 1, 13D).

The bank to river right is a densely-vegetated, gently sloping hill that transitions to a steep hillslope with exposed bedrock; downstream of the five bedrock steps, the border on river right is a cliff face with horizontal bedding. The bank to river left is the densely-vegetated narrow historic floodplain, which rises to a terrace now used for agriculture.

The channel is sediment-rich on river right throughout the entire study reach. River left is primarily exposed bedrock. Generally, sediment on river left is confined to the zone of backflow behind each bedrock step, where recirculating eddies form in low flow and likely remain in high flow when sediment is mobile. Beyond the backflow zone, flow "reattaches" to the bed and net flow is downstream, rendering the exposed bed largely void of sediment. In low flow (discharge ~150 cfs at the gauge), step 3 creates a hydraulic jump with a ~20 cm head difference between trough and crest.

In high flow, the hydraulic structures generated by step 3 amplify in size. A flashy precipitation event on 23 January, 2017 created a 3-foot increase water height at the gauge over six hours and generated a well-defined hydraulic jump and trailing chain of four well-defined standing waves (Fig. 11).

2. Methods

Preparation for this project involved multiple steps: selecting the data-logging electronics, extracting the bedrock block, building a waterproof capsule for electronics, 3D modeling the block, assembling electronics inside the capsule, and preparing the block to go out to the river. Setup for preliminary experiments will be discussed together with the results in the following section.

2.1 Data logging electronics

After a literature review and evaluation of current data-logging devices on the market, our research team decided that the most time- and cost-effective solution was to take a Do-It-Yourself approach. We modeled our components based on those used in ongoing studies for monitoring flow conditions in underwater caves (Mallon). Electronics consist of a Teensy 3.6 Arduino-compatible,16-bit data logger; 16-bit MPU6050 triaxial accelerometer/gyroscope with

six degrees of freedom; two MS5803-14BA fluid pressure sensor breakout boards; and a 3.7 V, 2200 mAh lithium-polymer battery (Fig. 12).

The MPU6050 is an inertial measurement unit (IMU) compatible with the I^2C Serial Interface. Every measurement consists of six simultaneously-recorded 16-bit integer data points, one for each axis of acceleration and rotation: a_X, a_Y, a_Z and g_X, g_Y, g_Z, respectively. The device runs on a 3.3V power supply. The accelerometer uses independent proof masses for each axis (InvenSense, 2013). Therefore, the device is able to detect acceleration (measured in gravitational units, g) on any of the three axes independently of the others. At rest, and when in standard orientation (labeled on the IMU), the device measures ~0 g on the X and Y axes and ~16,000 (1 g) on the Z axis. The gyroscope also uses separate detectors on each axis; it consists of three vibratory MEMS-rate gyroscopes to measure changes in angular rotation (deg/s) along the three axes. A data conversion of raw_data/32767*250 is required for the ±250 sensitivity instrument. During rotation, the Coriolis Effect causes detectable vibrations that are captured by a capacitive pickoff device to detect changes in device orientation. The signal is transformed and filtered on board, turned to a voltage, and then digitized by the 16-bit Analog-to-Digital Converters (ADCs).

The MS5803 pressure sensors also communicate with the I^2C Serial Interface. The sensors have an operating range of 0 to 14 bar and -40-85 °C, well within the range of what the sensors might experience in a river even in flood stage. The sensor records values as 4 byte floating point data.

The Teensy board is capable of reading programming sketches from various software and satisfies the physical size limitations of the waterproof housing (detailed in section *2.2*). It stores data on a 32-GB microSD card. We made minor modifications to existing Arduino libraries for the IMU and pressure sensors to ensure proper communication with the Teensy. Using these modified sensor libraries, a simple Arduino sketch (140 lines) was sufficient for logging the eight sensor values (six IMU values and two pressure sensor values) as 16-bit binary numbers at 40 Hz. At that rate, the 32-GB SD card can hold over 600 hours of log data—far greater than the approximately 24 hours of continuous power from the battery. When selecting sampling rate, we modified the Arduino sketch to display data values as text characters in real-time to a host computer over USB connection, allowing visualization and calibration of the sensors.

2.2 Block extraction

We extracted the block on July 21, 2016. I analyzed the crack network to find an area where block extraction would be achievable. I selected a bedrock slab that had three sides either pre-fractured or pre-exposed (Fig. 10). This setup thus required initiating one new crack. Having three natural, pre-existing cracks was ideal, as the goal was to keep the setting as natural as possible within the scope of the project as well as minimize the amount of manual labor required to remove the block from the surrounding bed. The selected block location is close enough to the bedrock step to feel effects of free surface undulations produced by high-flow hydraulic structures (Fig. 11C).

I thoroughly photographed the surrounding area using a waterproof GoPro HERO3 camera, starting at the lip of step 4 and walking upstream towards step 3. Sediment in cracks may indicate the presence of hydraulic jacking (Hancock et al. 1998). For ease of extraction, I removed as much sediment as possible using a rock hammer and brush. I also removed a cobble-sized, angular rock block that was acting as a chock to river-right of the block. I then used a 16-lb tamping bar, 48 in wrecking bar, rock hammer and mallet to crack out the block. The water was about 0.75 m deep (Fig. 13).

First, we used the tamping bar to etch an initial groove. We then switched to the wrecking bar for more efficient hammering. We also tried wedging the tamping bar underneath the slab to pry out the block from below; this method proved unfruitful and resulted in a stuck tamping bar. We found that the most effective method was wedging the pointed end of the rock hammer into the groove and striking the blunt end with the mallet. We moved the hammer along the groove to allow energy from each strike to propagate through the rock in all directions. After four hours, the rock cracked away from the surrounding bed. We wiggled it back and forth to liberate it from tightly wedged sediment. In addition, the rock cracked on a diagonal and it was hooked on its upstream end. We used the tamping and wrecking bars to lift the downstream end of the block and remove it from the bed (Fig. 13). The cracked surface was jagged and uneven due to the nature of the fracture.

To ensure that the block would be “pluckable” by the river, we chiseled the lip that remained on the intact upstream bedrock and also the upstream side of the block. We smoothed the edges of the two chock blocks—a second chock was cracked from the surrounding bedrock during extraction—to ensure that all pieces would fit together smoothly. After assuring that the

blocks would all fit together again, we transported the block back to the Washington and Lee University geology department. I used a 2-inch drill bit to remove a core from the rock. The resulting core hole was approximately 1.8 inches (4.6 cm) in diameter. This core hole set the size limitations for the waterproof housing for electronics.

2.3 Waterproof housing

The housing for electronics is a custom-designed, 3D-printed ABS plastic capsule designed using TinkerCAD and printed using the CatalystEX 4.5 software and Uprint 3D printer FMS (Flexible Manufacturing System). The housing is composed of two pieces: the barrel and slide (Fig. 14). The barrel has an outer diameter of 43 mm, inner diameter of 41 mm and height of 10.8 cm to conform to the dimensions of the block core hole (total capsule height reaches 11 cm when fully assembled with a rubber washer). Notched columns on either side of the inside of the barrel support the slide, and the columns themselves are the screw-attachment points. The bottom of the barrel has a rectangular cavity to hold one fluid pressure sensor. The cavity has a slot along its long axis to allow wires from the pressure sensor to enter the interior of the body of the barrel. Two grooves perpendicular to the long axis of the cavity hold metal wires that protect the ceramic diaphragm of the pressure sensor. An identical cavity is on the slide. The slide has a tongue on which the electronics are mounted. The data-logging equipment is on one side of the tongue and the battery is on the other. The slot at the top of the tongue allows the battery wires to pass from one side of the capsule to the other.

Performing waterproofing tests required partial assembly of electronics. To assure impermeability of the capsule, I first installed the fluid pressure sensors. I removed any dust from the capsule using compressed air. I rolled out a small bit of epoxy putty and wrapped it around the point of wire connection to pressure sensor. Upon placing the wires through the slot and the pressure sensor in the cavity, the excess putty oozed through the slot to the underside. I smoothed the putty on the underside of the cap to ensure complete closure of the slot. After the putty cured, which secured the sensors in place, I mounted the sensors in clear, marine-grade Loctite EA E-30CL epoxy, careful to only cover the electronic board and leave the ceramic pressure-sensing diaphragm exposed (adapting electronic-mounting methodology from Mallon). At the same time, I mounted rigid metal wires in the grooves so all parts requiring epoxy could

harden concurrently and ensure cohesive curing among all components. The metal wires intend to protect the ceramic diaphragm from any impacting sediment.

With the pressure sensors in place (but not the rest of the electronics), I could test the waterproofness of the sealed capsule. I evaluated moisture entry using delicate lab-grade tissues to detect even the slightest moisture content. Initial waterproofing attempts included various combinations of o-rings, screws, silicon cement and rubber grease to create an impervious seal. At first, the capsule was not water-tight and an amount of water that would cause electronic shorts had leaked inside. Random moisture distribution within the capsule suggested that water entry was not limited to the screw points or the point of contact between the barrel and slide pieces. I disassembled the capsule and filled the barrel with water. Water traveled through the walls of the plastic and appeared as droplets on the outside. To correct this flaw, I painted the capsule with acetone (Draper, 2016). Acetone melts the plastic enough that micropores and other imperfections are eliminated but the overall, larger structure is not compromised. I repeated the test of filling the barrel with water and let it stand for 4 hours. No water leaked through, suggesting that the acetone paint was successful at sealing the pores.

Another series of failed waterproofing tests using combinations of o-rings, closed-cell neoprene foam, rubber grease and silicon cement resulted in trying a new material for sealing the capsule. A flat rubber washer, cut from a 1.5-mm-thick sheet of flat rubber, created a successfully waterproofed seal between the barrel and slide. I cut the rubber washer to mirror the shape of the inside of the barrel. The flat rubber ensured uniform compression of the washer. Non-uniform compressibility was an issue identified with the o-ring; the two screws over-compressed the o-rings near the screws and under-compressed the o-ring 90 degrees between the screws. The flat washer corrected this issue. The washer also extends inside of the capsule to cover the screw holes, adding extra protection against water entry at the screw sites.

To ensure no leakage through the screw sites, I also applied silicon sealant around the screws at the final stage of inserting the screws into the capsule. The sealant cures to a flexible solid that prevents water from entering the screw sites but does not restrict removal of the screws for re-opening the capsule after tests.

2.4 3D modeling/photogrammetry

To aid determination of the physical properties of the block, such as volume, I used Structure from Motion photogrammetry to build a 3D digital model of the rock. This required scrubbing the block clean of moss and algae and transferring it to a suitable facility for photography. At the Washington and Lee University's Integrative and Quantitative Center, I placed the rock on its z-axis on a table atop white paper with multiple, distinct control points. I photographed it from three angles (low, zero and high angle), 360 degrees around the block. Three lights illuminated the block to minimize shadows. I used a Nikon D610 Single-lens reflex digital camera linked remotely to one of the lights; capturing a photo triggered one of the lights to flash and the other two lights to flash upon detection of the first.

I set the camera focus once for the entire session by standing about 3 feet away from the rock and focusing the lens to the center of the rock. In order to maintain the focus setting, I found the appropriate distance from the block for each new photo location by moving the whole camera rather than adjusting the lens. I took about 20-25 photos in each circle around the rock. I then flipped the rock 180 degrees and repeated the photography process.

I transferred the raw photos to a computer and edited them in Bridge software to correct the lighting of the photos. I adjusted the exposure to +0.70, shadows to +18 and blacks to +14 while keeping all other settings default. I converted the photos to .jpg files and resized the width to 3000 pixels.

Using Agisoft Photoscan, I built two separate "chunks", one for the top half of the rock (first round of photos) and one for the bottom half (second round of photos). I added and then aligned the photos before building a dense cloud. I inserted 12 points on the dense cloud and assigned real-world distances so the program could scale the image. To verify that the program could accurately predict linear measurements, I entered four additional points on the dense cloud and instructed the program to predict the distance between points. I verified predicted values by measuring real-world distances between the same points on the real block. The values were accurate to mm precision.

I then merged the two dense cloud chunks to make one enclosed model of the rock. I first removed all extraneous pixels that represented other surfaces in the photographs, particularly the table that the block sat on during photography. I followed standard steps for building a model. I then rechecked Photoscan's ability to make estimated measurements of linear distances on the

rock. The measurements had an accuracy of 0.001 m. With confidence that Photoscan was able to make measurements, I used the 3D model to determine a block volume of 9353 cm^3 (Fig. 15).

2.5 Electronics assembly

Preliminary configuration and assembly of electronics involved mounting a Teensy data logger on a breadboard and soldering the rest of the electronics to it (Fig 16). This enabled us to start data programming and ensuring that all electronics could communicate before installation into the capsule. I used the breadboard setup to gather preliminary movement data in order to understand the signal signatures associated with specific movements (detailed in section *3.1*). Initial assembly also allowed me to determine the lifetime of the battery. A charged battery will power the device for approximately 24 hours regardless of sampling rate (battery life tested with sampling rates of 20, 40 and 100 samples/sec). I selected 40 samples/sec as the sampling rate to use for experiments because that rate provides a good signal:noise ratio. After achieving satisfactory results from the breadboard assembly, we moved on to installing the electronics in the capsule.

I planned and executed a series of soldering steps to ensure that the various electronic components could all fit into the capsule with minimal excess wire (Fig. 17). I first attached the IMU to the Teensy. Before mounting the pieces together, we made two solders using 24 AWG single-strand connection wires for the GND (ground) and 3.3V (power) to the IMU. We inserted a dab of hot glue between the wires to act as extra insulation and prevent shorting. I then soldered two header pins to create a rigid mount connection between the IMU and Teensy. For additional support, I used two pieces of 1-mm-thick double-stick tape to mount the IMU to the computer component of the Teensy. I then measured the distance required to attach the wires to the corresponding ports on the Teensy (I^2C bus 0, pins 18 and 19). After identifying the appropriate wire length, I shaved away the insulating plastic to expose the wires. I then soldered the wires to the Teensy from the backside of the Teensy.

Next I attached the battery wires to the Teensy. These wires attached to the V_{in} and GND ports at the USB-port end of the Teensy. Next, I connected the wires bridging the bottom pressure sensor to the Teensy. The ground and power wires connected to the Analog GND and 3.3V ports at the USB-end of the Teensy, respectively. The SLC and SDA wires connected to ports 3 and 4 (I^2C bus 2), respectively. This step involved preserving the length of the wires as

much as possible. The length of the wires from the bottom pressure sensors to the electronics limits the extent to which the barrel and slide can be separated (Fig. 17D, F). Maintaining the maximum length helped make assembly and re-assembly easy.

The final soldering step was to connect the top pressure sensor to the electronics. I carefully measured where on the tongue to mount the Teensy in order to minimize excess wire but still provide enough length with which to work. The challenge in this last step was that I could not mount the Teensy on the tongue until after soldering; otherwise I would not have been able to access the ports to apply the solder and make a strong connection between wire and pin. This complication meant that I had to be extremely careful in trimming wires. We made the final solder, connecting the ground and power wires to the GND and 3V ports located just above the Teensy reset button, and the SCL and SDA wires connected to ports 37 and 38 (I^2C bus 1), respectively. I then used double-stick tape to secure the Teensy to the tongue, and assembly was complete.

It is important to note the orientation of the MPU in the device (Fig. 18). The sensor is positioned vertically but its factory settings are intended for horizontal arrangement. This places the MPU axes in an orientation where the y-axis is in the cross-stream direction (positive y corresponds to river left), the x-axis is in the vertical direction (positive x corresponds to down-direction; negative x values correspond to up-direction), and the z-axis is parallel to the flow direction (positive z is downstream, negative z is upstream).

Between each soldering stage, we checked for electrical shorts by powering the device and using a BK Precision 2704C multimeter. Absence of electrical shorts allowed us to proceed. After completing the full assembly, we used the serial monitor function in the Teensyduino program to ensure that the device still read data correctly.

2.6 Final block preparation

Before returning the block to the river, I spray-painted it neon green to help identify it in the river. In low water, the green block can be seen from the bank while it is sitting out in the hole, and presumably it will be easily recovered should it pluck.

3. Results of Experiments

3.1 Breadboard test

Flume studies by Wilkinson et al. (2015) revealed various movement patterns plucked blocks take upon lifting out of the bed. Based on these findings, I simulated block motions with the breadboard setup to gather preliminary data to plot in Matlab and understand how the various sensors detect each type of movement. I secured the breadboard assembly to a metal bookend in the approximate orientation the device would have when emplaced in the block (Fig. 16). I simulated rotation, in-place vibration, direct vertical lift, and downward settling. I video recorded the experiment in order to correlate the data with timing of movement (S1, Vid. 1).

The sensor created signals that are readily interpreted for both acceleration and gyroscope data (Fig. 19). I did not analyze pressure sensor data because both sensors were simply recording air pressure. I first imitated a fulcrum-style rotation in the downstream direction. The overall device movement was upward and in the simulated downstream direction, followed by a return to neutral. The IMU sensor is located in the middle of the MPU device. As it is rotated, the center experiences a tilt that moves the center backwards and down. This is reflected in the data by a negative trend in z (backward movement) and a positive value in x (downward movement). Cross-stream acceleration is subdued compared to the other two axes and is result of an unsteady hand—I did not intentionally move the assembly in the cross-stream direction. Rotation values up to ±250 deg/sec reflect the varying speeds with which I moved the assembly (Fig. 19). Gyroscope data is consistent with the acceleration data. The device was pivoting around the cross-stream axis and the graphical response is greatest for that axis. Rotation about the other two axes is minimal.

In-situ vibration is displayed as a low-signal response from all three axes of both the accelerometer and gyroscope. The signal is lowest for acceleration in the vertical direction, a result of not lifting the device off the table very far.

Vertical lifting returns the greatest signal in the accelerometer's vertical axis. Keeping in mind that negative x-values correspond to vertical lift, the initial response is a negative peak followed by a positive peak, and then returns to ~0, representing a return to a neutral position on the table. I varied lift speed and maximum height. The breadboard test was a successful proof of concept exercise and also provided a baseline dataset to which I can compare the results of other experiments.

3.2 Wet tests

I conducted two "wet tests" to investigate the performance of the electronics in water. The first test was a simple submersion of the capsule in a 1.5-m-tall PVC pipe filled with water. The second test was a "controlled" river test, in which I placed the rock back in its excavation site and introduced upstream flow obstructions to alter flow and create turbulence over the block. I then conducted the first 24-hour-long river experiment.

Still-water test

The still-water experiment tested pressure sensor sensitivity to changes of depth. It also served as a trial of how to start the data logger and close the capsule as quickly as possible. To gather data about how the pressure sensors react to changing depths and hydrostatic pressure head, I secured a weight 30 cm below the capsule and a measuring tape 10 cm above it. I then used the measuring tape to lower the apparatus down into a 2.05-m-tall, narrow 2.5-in-wide PVC pipe filled with water (Fig. 20). I allowed the capsule to sink to the bottom via its own weight; once it reached the bottom, I brought it back up by pulling on the measuring tape in increments of 10 cm and varying speeds.

I was most interested in analyzing pressure sensor data from this experiment (Fig. 21). In air, both pressure sensors read approximately zero m H_2O (1 m $H_2O \approx 0.01$ atm). As the capsule descended in the pipe, pressure head increased slowly to a maximum of 1.7 m H_2O. This height reflects a distance of 30 cm between the capsule and the bottom of the pipe. After about 10 seconds, I pulled the capsule up in increments of 10 cm, varying speed with each pull. The pressure sensor data reflects the varying rates of lift; speed of lift is seen in the slope of the pressure data between flat lines (Fig. 21). The data accurately record the height of the overhead water column. Moreover, the top and bottom pressure sensors consistently show a difference in about 0.1 m H_2O, due to the 11 cm height of the capsule. Acceleration and rotation data are minimal but show movement in and around the vertical axis with each lift.

River test

The river test was the first time that I installed the capsule in the rock. To do this, I used silicon sealant to hold the capsule in place. I first threaded a thin metal wire through the hole and secured it at the front of the block to assist with post-test capsule removal. I then inserted the capsule. I squeezed sealant onto the capsule and twisted it while pressing it into the hole. Twisting the capsule dragged sealant inside the hole and filled the space between the capsule and

rock. I put an extra layer of sealant around the perimeter of the capsule on both the bottom and top of the rock, smoothing it down to ensure a flat seal. I used this same methodology whenever I returned the block to the river.

This test intended to reveal the way the pressure sensors and IMU read in relatively low-water conditions. I assembled the block in the laboratory and then transported it to the field site. I placed the block in the hole, let it sit in natural channel flow for about 15-20 minutes, and then conducted some "controlled" experiments in which I introduced an upstream obstacle to generate turbulence above the block (S1, Vid. 2). An assistant and I lowered a plywood board into the flow at the upstream end of the block hole (Fig. 22). We let the board rest on the bed for about 5-10 seconds, and then lifted the board quickly. We repeated this procedure three times. We repeated the same procedure another three times at a distance nearly 0.5 m upstream of the block.

The data from this experiment were perplexing in many ways. Most notably, the top pressure sensor recorded data with much greater fluctuations than the bottom pressure sensor (Fig. 23). Moreover, the pressure sensors in this test have the same average reading of water depth. According to the reliable results of the still-water test, the pressure sensors should show a head difference of ~0.110 cm due to the difference in hydrostatic pressure. The cause of these perplexities is unknown.

Despite complications from this experiment, the data did reveal patterns in pressure readings that reflect the influence of introducing an obstruction to the flow. When I lowered the plywood board into the flow, pressure recordings increased (Fig. 24). Lifting the board initiated an increase in flow velocity across the block surface, reflected as a drop in both top and bottom pressure data. Three iterations of lowering and raising the board close to the block are represented by quick changes in pressure while the three iterations performed farther upstream are represented by slower changers in pressure. The introduced turbulence was insufficient to cause block movement.

At t = 9710 sec, the pressure sensors adjust to show the expected ~0.110 m H_2O difference in pressure. I did not do anything to the block to which I can attribute this adjustment.

24-hour experiment

The 24-hour experiment intended to capture as much of the rising limb of a storm hydrograph as possible, and therefore required quick action to deliver the instrumented block to the river. On March 01, 2017, I took the block to the river site before a predicted storm. I

assembled the electronics in the laboratory and started a stopwatch immediately after connecting the battery to the device. I also took note of the clock time. I did this in order to have an absolute time to which I could compare the data logger recordings during analysis, and from which I could verify a sampling rate of 40 samples/sec.

Upon reaching the river, I carried the block to the river bank and left it on shore while I measured water depth above the bed just upstream of the hole (depth = 0.67 m). I then dragged the rock out to the hole in a plastic crate. The first signal in the data corresponds to this movement, which was timed perfectly with the stopwatch for ease of data/time correlation (Fig. 25). When I took the rock out of the crate, I placed it on the bed just downstream of the hole and aligned it with the hole. To address the concerns from the river test, I performed a series of block rotations and flips to have specific sensor data signals that I could later correlate to recorded times of movement. First, I rotated the block clockwise three times at increments of 90°, recording the time of each rotation. I then flipped the block upside down and rotated it again, still recording the time of each movement. I then re-righted the block and placed it down in the hole, making sure that it was level with the surrounding bed. Lastly, I placed my hand over the top pressure sensor. This action, as well as the rotations, were performed to have specific events of sensor data for better data evaluation.

To examine the extent to which flow exchange from the sub-bed to channel flow exists, I inserted a porous plastic baggie filled with blue dye into the space between the block and the upstream bed. I prodded the baggie to release the dye and watched it escape into the flow (S1, Vid. 3). At times, the dye would linger in the crack, protected by the bed and block from the channel flow. At other times, the dye would be quickly whisked upwards into the channel flow. After completing this exercise, I left the block in the water to record data until the battery ran out, which was about 22 hours.

Data from this experiment clearly shows the different iterations of rotating and flipping the block (Fig. 25). All data show a unique response to movement, and the top and bottom pressure sensors always show a hydrostatic head difference of about 0.1 m. Most notably, after the block is transferred to the hole, the top pressure sensor records approximately the same value that the bottom pressure recorded when the block sat on the bed.

Rainfall during this event was less than predicted and did not result in a significant rise in gauge height. From the time the block went into the river about 2 pm on March 01 to when the

battery ran out and data recording ceased about 9 am on March 02, water height at the downstream gauge only increased 0.13 ft (0.04 m), from 1.82 ft to 1.95 ft. Discharge at the gauge increased from 174 cfs to 214 cfs. This change of stage was not great enough to induce any block movement. Acceleration and gyroscope data returned a flat response (Fig. 26). The pressure data is also rather flat-lying, but careful examination shows a slight increase in pressure with time (total $\Delta = 0.012$ m), reflecting a small but real rise in water height. A few signals in the data reflect changes in water height four hours after data logging began, nearly two hours after I left the block unattended in the river (1.55×10^4 seconds, Fig. 27). Without film footage of river activity, it is difficult to conclude what these oscillations might imply, especially because these oscillations happened more rapidly than what the downstream gauge would record (gauge sampling rate = 15 minutes).

Fine-scale analysis of the pressure readings from this experiment reveals that there might be a regular undulation of flow pressure that operates on the order of seconds (Fig. 28). Some signal pairings (same-colored circles) have similar changes in pressure at slightly different times (red, green) while other signals occur at roughly the same time but show different magnitudes of pressure change (orange, yellow, blue). No change of rotation or acceleration accompanies these pressure variations.

4. Discussion

An uncharacteristically dry springtime for southwestern Virginia prevented me from capturing a flashy flood event with the instrumented block. It is therefore valuable to understand what sorts of flow conditions will lead to plucking. Hancock et al. (1998) suggest when lift overcomes the block normal force, plucking will occur (Fig. 3). Wilkinson et al. (2015) found that model bedrock blocks can remain on the bed while they are neutrally buoyant. The blocks vibrate in place until some transient event drives plucking. Harbor et al. (in prep) determined that blocks will pluck under a head difference of 4-10 times the head required to reach neutral buoyancy. The study block has an effective normal force of 163.37 N over a basal area of 850 cm^2, which corresponds to a head of 0.20 m to reach neutral buoyancy (A1). Therefore, it is possible that this block could pluck starting with as little as 0.80 m of head change. Assuming that the hydraulic jump grows proportionally to change of stage, the jump reaches 0.80 m with 14.01 ft (4.27 m) of depth at the study site (Eq. 1).

$$\frac{0.35\ m\ jump}{6.13\ ft\ at\ study\ site} = \frac{0.80\ m\ jump}{x\ ft\ at\ study\ site} \quad \text{Eq. 1}$$

Stage of 6.13 ft comes from gauge data during the January 23 event and corresponds to an observed jump height of 0.35 m (Fig. 11). I assume that stage does not change significantly from the study site to the gauge. This simple ratio implies that a jump of height 0.80 m corresponds to a stage of 14.01 ft and a gauge discharge of 12130.14 cfs. Elium (2015) calculated a gauge:study site discharge ratio of 1:0.54 that I used to determine the minimum study site discharge required to pluck the block. This discharge is ~6530 cfs, which falls between the peak discharge values (cfs) expected for 2- and 5-year floods at the study site (Elium, 2015). Thus, this discharge has a >20% but <50% chance of occurrence each year, and hence, block plucking.

If the block were to pluck, I am confident that the electronics would record the event. The electronics are capable of detecting minor changes of pressure and movement, as indicated by the results of all wet tests. Results from the board experiments suggest that the pressure sensors capture changes of flow turbulence and are sensitive to proximity of flow-altering features. Based on wavelengths of pressure recording oscillations, it is possible that I can determine relative location of hydraulic structures in future experiments—if oscillation wavelengths are small, the structure is likely close to the block but if wavelengths are larger, the structure is likely farther upstream. Pressure fluctuation trends reveal a detectable pattern, yielding the river test a valuable exercise. Although this facet of the data was informative, potential error with the top pressure sensor amplitude and the same average readings for both sensors render the data unreliable for determining absolute pressure values. To a degree, increased noise should be expected for the top sensor because it is exposed to free channel flow while the bottom sensor is sheltered at the bottom of the hole. However, our hypothesis that dynamic sub-bed flow constantly exchanges with channel flow would be nullified if the amplitude of pressure recordings truly differs as much as the first test data suggests. Moreover, the same average reading for both sensors implies that somehow the effect of hydrostatic pressure was eliminated, which is a violation of fluid mechanics. A possible explanation for the radical data could be a short in the electronics or difficulty adjusting to the cold temperatures of the river, even though the temperature was within operating range of the sensors; the latter is thus a minor likelihood.

The 24-hour experiment returned a flat response, but I expected that response because little precipitation occurred. The stage rise of 0.012 m detected by the pressure sensors indicates their sensitivity. The dye exercise revealed that sometimes crack network flow lingers around the block and sometimes it is rapidly mixed with the channel flow above. These observations likely suggest that flow exchange between the channel and the sub-block crack network does occur, and operates in pulses of no to intense exchange over random time intervals. Moreover, pressure fluctuations on the order of seconds indicate that flow both above and below the block feels the effect of turbulence, but the responses are either different in timing or amplitude (Fig. 28). Observations from the dye exercise and sensor recordings suggest that dynamic flow exchange between cracks and the sub-bed with channel flow exists even in low-discharge, subcritical flow. This exchange therefore does not require a well-developed plunging jet like those used in studies by (Federspiel et al., n.d.), although the exchange is likely enhanced in the presence of stronger structures. The plywood board tests in the river test also show evidence of exchange between the sub-bed and the channel flow. As we lifted the board and flow velocity across the block increased, fine-grained sediment was sucked out from underneath the block and transported by the channel flow.

The presence of sediment beneath the study block is intriguing in its own right. Wilkinson et. al (2015) observed that bubbles and model bedrock blocks slide upstream in the flume. They proposed that the mechanism driving this process is a pressure gradient caused by hydraulic structures. It is plausible that flow in natural channels also has a pressure gradient that can draw sediment upstream towards areas of lower pressure. The block hole is approximately 1.5 m upstream of the lip of the bed and is underlain by sediment, some of which is cobble-sized. The only route the sediment could have taken to arrive at that position was underneath the bed. We believe that the sediment-filled zone beneath the sandstone bed was formerly a shale layer that eroded away. It is plausible that when the shale weathered and eroded, sediment filled the eroded space below the sandstone bed. The pressure gradient produced by the step 3 hydraulic structures likely causes a pressure gradient sufficient to move sediment upstream. This discovery alone merits further investigation.

Much future work remains for this study. The groundwork for data collection and interpretation is complete, but a more robust dataset would greatly enhance our understanding of plucking in natural settings. Extending battery life would greatly benefit this study; 24 hours is

likely insufficient for capturing both the rising and falling limbs during a storm event. Remote data collection via Bluetooth connections might also benefit the study by allowing the PI to be at the river, witnessing the flow and seeing the data in real-time.

5. Conclusion

The electronics used in this study detect changes in pressure and movement with great sensitivity and will likely return reliable data in future studies. Monitoring plucking in natural channels is replete with challenges; when plucking is most likely to occur, it is too dangerous to witness the process in the channel itself. Remote monitoring of bedrock blocks might alleviate some of the challenges in detecting the plucking mechanisms.

Several factors that may enhance the likelihood of plucking include proximity of a target block to a hydraulic structure (Harbor et al., in prep), strength—head difference—of the hydraulic structure (Harbor et al., in prep), and influence of weathering agents such as sediment wedging and chemical weathering expand the crack network (Snyder et al., 2003; Li et al., 2016). Though protrusion of a target block into the flow is not required for block uplift, it may assist the process (Coleman et al., 2003; Lamb et al., 2015; George et al., 2015). If it were possible to instrument more blocks in the field, trying different scenarios will help the development of a plucking rate law.

Non-flood discharge of the Cowpasture River is insufficient to pluck the study block. The discharge required to do this, ~6230 cfs, is slightly less than double the peak discharge for the past calendar year. It is possible that a flood this large could happen with the likelihood equal to or less than that of a 5-year flood.

References

Annandale, G.W., 2005, Scour technology: mechanics and engineering practice: McGraw Hill Professional.

Barnes, H.L., 1956, Cavitation as a geological agent: American Journal of Science, v. 254, p. 493–505, doi: 10.2475/ajs.254.8.493.

Beer, A.R., Turowski, J.M., Fritschi, B., and Rieke-Zapp, D.H., 2015, Field instrumentation for high-resolution parallel monitoring of bedrock erosion and bedload transport: Earth Surface Processes and Landforms, v. 40, p. 530–541, doi: 10.1002/esp.3652.

Benelli, G., Pozzebon, A., Raguseo, G., Bertoni, D., and Sarti, G., 2009, An RFID Based System for the Underwater Tracking of Pebbles on Artificial Coarse Beaches, *in* 2009 Third International Conference on Sensor Technologies and Applications, p. 294–299, doi: 10.1109/SENSORCOMM.2009.52.

Bertoni, D., Sarti, G., Benelli, G., Pozzebon, A., and Raguseo, G., 2012, Transport trajectories of "smart" pebbles on an artificial coarse-grained beach at Marina di Pisa (Italy): Implications for beach morphodynamics: Marine Geology, v. 291–294, p. 227–235, doi: 10.1016/j.margeo.2011.08.004.

Chatanantavet, P. and Parker, G., 2009, Physically based modeling of bedrock incision by abrasion, plucking, and macroabrasion: Journal of Geophysical Research F: Earth Surface, v. 114, http://www.scopus.com/inward/record.url?eid=2-s2.0-77954239662&partnerID=40&md5=516aae5184355e9c6e7e77db7dc7cf56.

Chen, G., Schafer, B.P., Lin, Z., Huang, Y., Suaznabar, O., Shen, J., and Kerenyi, K., 2015, Maximum scour depth based on magnetic field change in smart rocks for foundation stability evaluation of bridges: Structural Health Monitoring, v. 14, p. 86–99, doi: 10.1177/1475921714554141.

Coleman, S.E., Melville, B.W., and Gore, L., 2003, Fluvial entrainment of protruding fractured rock: Journal of Hydraulic Engineering, v. 129, p. 872–884, doi: 10.1061/(ASCE)0733-9429(2003)129:11(872).

Dubinski, I.M. and Wohl, E., 2012, Relationships between block quarrying, bed shear stress, and stream power: A physical model of block quarrying of a jointed bedrock channel: Geomorphology, v. 180–181, p. 66–81, doi: 10.1016/j.geomorph.2012.09.007.

Elium, E., 2015, Field and Flume Exploration of Channel Bedrock Erosion by Plucking: Washington and Lee University, 44.

Federspiel, M.P.E.A., 2011, Response of an Embedded Block Impacted by High-Velocity Jets:, doi: 10.5075/epfl-thesis-5160, urn:nbn:ch:bel-epfl-thesis5160-3.

Federspiel, M.P.E.A., Bollaert, E.F., and Schleiss, A.J., 2011, Dynamic Response of a Rock Block in a Plunge Pool due to Asymmetrical Impact of a High-velocity Jet (PDF Download Available): Engineers Australia, p. 2404–2411.

Federspiel, M.P.E.A., Bollaert, E.F., and Schleiss, A.J., n.d., Experiments on the reponse of a rock block in a plunge pool loaded by a symmetrical jet impact:

Fiorotto, V. and Rinaldo, A., 1992, Fluctuating Uplift and Lining Design in Spillway Stilling Basins (abstract): Journal of Hydraulic Engineering-Asce, v. 118, p. 578–596, doi: 10.1061/(ASCE)0733-9429(1992)118:4(578).

Freeman, J., 2016, Evidence of Plucking at Balcony Falls on the James River, Virginia: Washington and Lee University, 42 p.

George, M.F., Sitar, N., and Sklar, L., 2015, Experimental Evaluation of Rock Erosion in Spillway Channels, *in* ARMA, American Rock Mechanics Association, v. ARMA 15-700, p. 6.

Gronz, O., Hiller, P.H., Wirtz, S., Becker, K., Iserloh, T., Seeger, M., Brings, C., Aberle, J., Casper, M.C., and Ries, J.B., 2016, Smartstones: A small 9-axis sensor implanted in stones to track their movements: CATENA, v. 142, p. 245–251, doi: 10.1016/j.catena.2016.03.030.

Hancock, G.S., Anderson, R.S., and Whipple, K.X., 1998, Rivers over rock; fluvial processes in bedrock channels, *in* Tinkler, K.J. and Wohl, E.E. eds., Beyond power; bedrock river incision process and form, Washington, DC, United States, American Geophysical Union, p. 35–60, http://ezproxy.wlu.edu/login?url=http://search.ebscohost.com/login.aspx?direct=true&db=geh&AN=1999-018827&site=ehost-live.

Harbor, D.J., Wilkinson, C., Helgans, E., and Kuehner, J.P., in prep, Initiation of plucking in rapidly varied flow: Geosphere,.

Harbor, D.J., Wilkinson, C., Helgans, E., and Kuehner, J.P., 2015, Mechanisms and Rates of Plucking of Experimental Bedrock Blocks, American Geophysical Union Fall Meeting, San Francisco, CA, AGU, v. EP21A–0888.

InvenSense, 2013, MPU-6050 | InvenSense:, https://www.invensense.com/products/motion-tracking/6-axis/mpu-6050/ (accessed March 2017).

Lamb, M.P. and Dietrich, W.E., 2009, The persistence of waterfalls in fractured rock: Bulletin of the Geological Society of America, v. 121, p. 1123–1134, doi: 10.1130/B26482.1.

Lamb, M.P., Finnegan, N.J., Scheingross, J.S., and Sklar, L.S., 2015, New insights into the mechanics of fluvial bedrock erosion through flume experiments and theory: Geomorphology, v. 244, p. 33–55, doi: 10.1016/j.geomorph.2015.03.003.

Li, K.-W., Pan, Y.-W., and Liao, J.-J., 2016, A comprehensive mechanics-based model to describe bedrock river erosion by plucking in a jointed rock mass: Environmental Earth Sciences, v. 75, p. 517, doi: 10.1007/s12665-015-5113-0.

Mallon, E. Arduino based underwater sensors: Arduino based underwater sensors, https://edwardmallon.wordpress.com/ (accessed March 2017).

Molnar, P., Anderson, R.S., and Anderson, S.P., 2007, Tectonics, fracturing of rock, and erosion: Journal of Geophysical Research F: Earth Surface, v. 112, doi: 10.1029/2005JF000433.

Pan, Y.-W., Li, K.-W., and Liao, J.-J., 2014, Mechanics and response of a surface rock block subjected to pressure fluctuations: A plucking model and its application: Engineering Geology, v. 171, p. 1–10, doi: 10.1016/j.enggeo.2013.12.008.

Sklar, L.S. and Dietrich, W.E., 2004, A mechanistic model for river incision into bedrock by saltating bed load: Water Resources Research, v. 40, p. W063011–W0630121.

Snyder, N.P., Whipple, K.X., Tucker, G.E., and Merritts, D.J., 2003, Importance of a stochastic distribution of floods and erosion thresholds in the bedrock river incision problem: Journal of Geophysical Research B: Solid Earth, v. 108, p. ETG 17-1-17-15.

Stephenson, W.J. and Abazović, A., 2016, Measuring Coastal Boulder Movement Under Waves Using Tri-Axial Accelerometers: Journal of Coastal Research, p. 607–611, doi: 10.2112/SI75-122.1.

Tinkler, K.J. and Wohl, E.E., 1998, Rivers over rock; fluvial processes in bedrock channels, *in* Tinkler, K.J. and Wohl, E.E. eds., A primer on bedrock channels, Washington, DC, United States, American Geophysical Union, p. 1–18, http://ezproxy.wlu.edu/login?url=http://search.ebscohost.com/login.aspx?direct=true&db=geh&AN=1999-018824&site=ehost-live.

USGS Mineral Resources State geologic map compilation: interactive map: USGS Mineral Resources, https://mrdata.usgs.gov/geology/state/map.html?x=-78.8464152525638&y=37.5165737850333&z=7 (accessed March 2017).

Wende, R., 1999, Varieties of Fluvial Form, *in* Miller, A.J. and Gupta, A. eds., Boulder bedforms in jointed-bedrock channels, United Kingdom, IAG: John Wiley & Sons, p. 189–216, http://ezproxy.wlu.edu/login?url=http://search.ebscohost.com/login.aspx?direct=true&db=geh&AN=2001-015557&site=ehost-live.

Whipple, K.X., 2004, Bedrock rivers and the geomorphology of active orogens: Annual Review of Earth and Planetary Sciences, v. 32, p. 151–185, doi: 10.1146/annurev.earth.32.101802.120356.

Whipple, K.X., Hancock, G.S., and Anderson, R.S., 2000, River incision into bedrock: Mechanics and relative efficacy of plucking, abrasion, and cavitation: Bulletin of the

Geological Society of America, v. 112, p. 490–503, doi: 10.1130/0016-7606(2000)112<490:RIIBMA>2.0.CO.

Whipple, K.X., Snyder, N.P., and Dollenmayer, K., 2000, Rates and processes of bedrock incision by the Upper Ukak River since the 1912 Novarupta ash flow in the Valley of Ten Thousands Smokes, Alaska: Geology, v. 28, p. 835–838.

Wilkinson, C., Helgans, E., Harbor, D.J., and Kuehner, J.P., 2015, Mechanisms and Rates of Plucking of Experimental Bedrock Blocks, Geological Society of America Fall Meeting, Baltimore, MD, GSA.

Willett, S.D., 1999, Orogeny and orography: The effects of erosion on the structure of mountain belts: Journal of Geophysical Research: Solid Earth, v. 104, p. 28957–28981, doi: 10.1029/1999JB900248.

Figures

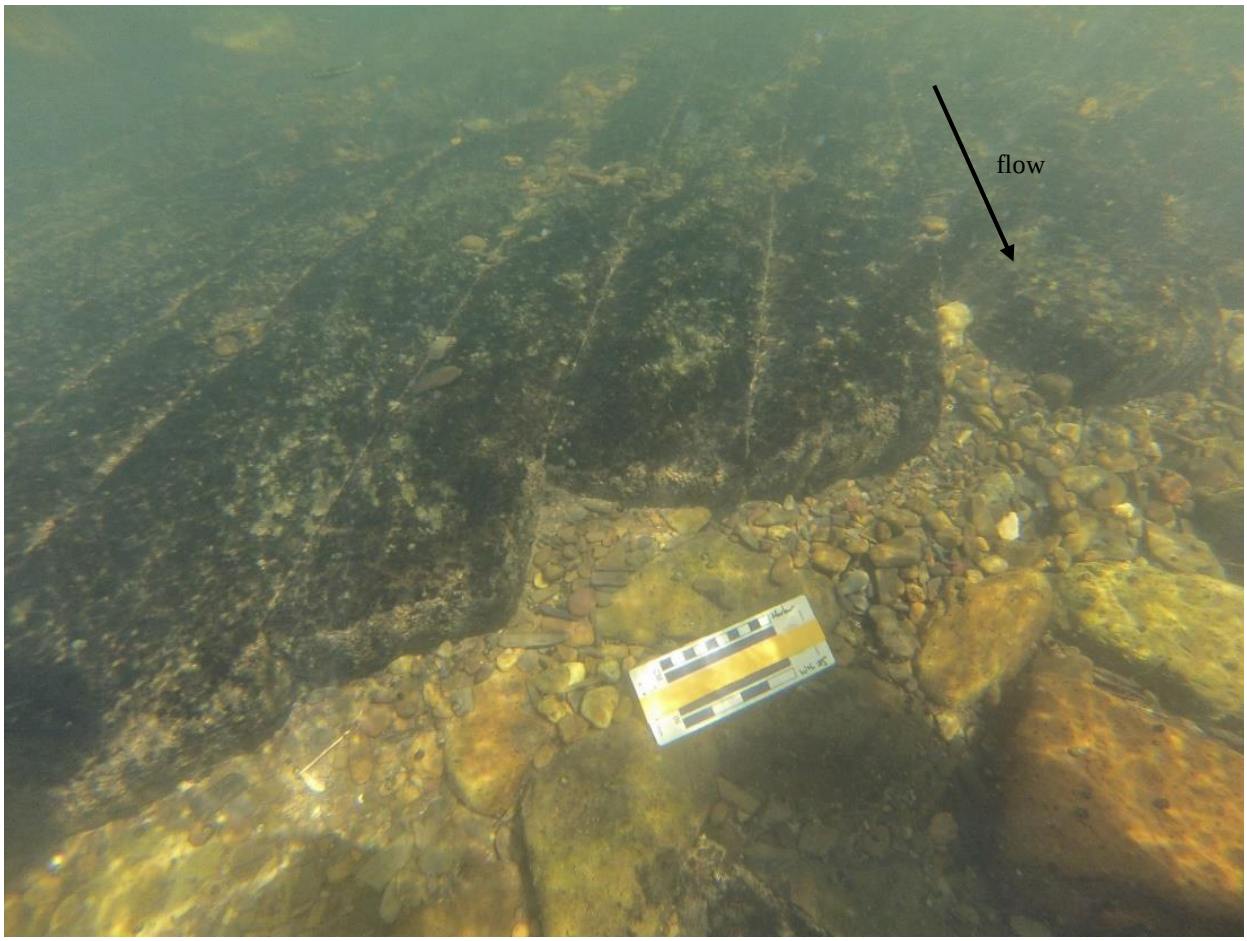

Figure 1. Evenly-jointed bedrock slab of homogenous, flat-lying Brallier sandstone. Sediment has accumulated below the lip of the bed. Scale is 10 cm on top bar.

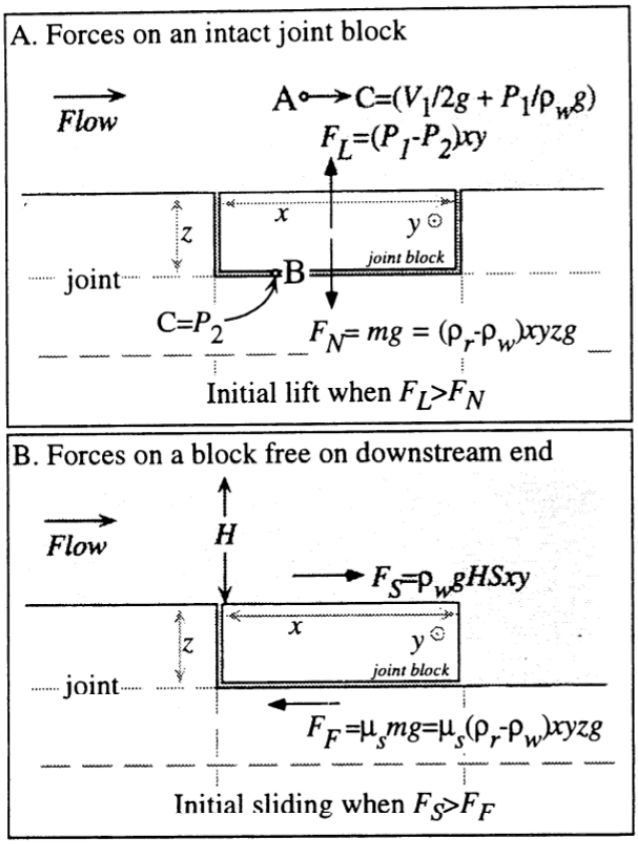

Figure 2. Forces acting on a block to initiate plucking by A) lift or B) sliding. (Hancock et al., 1998)

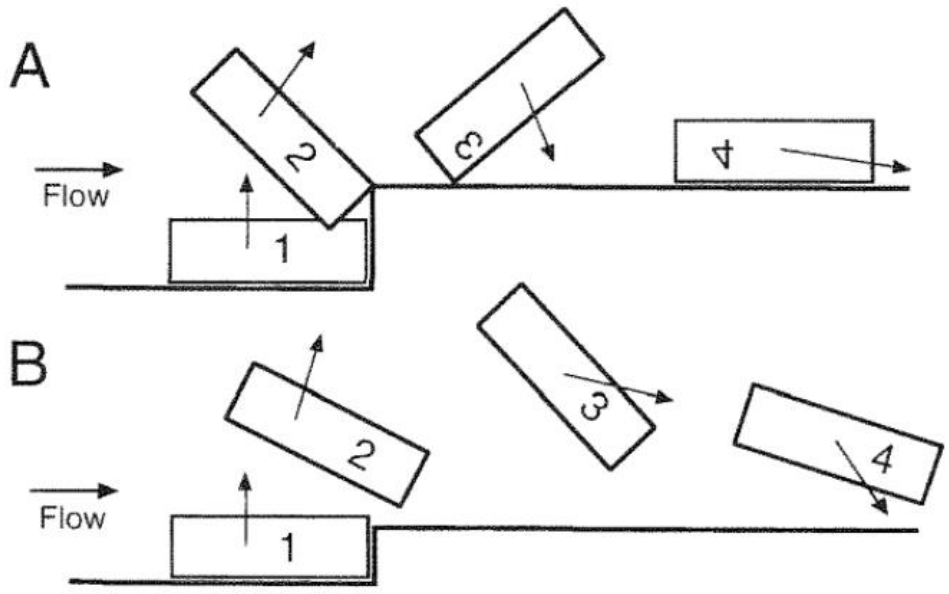

Figure 3. Schematic of two possible movement patterns for plucked blocks. A) Rotating around a downstream step. B) Lifting out of the bed and "floating" back down without rotation. (Wende, 1999)

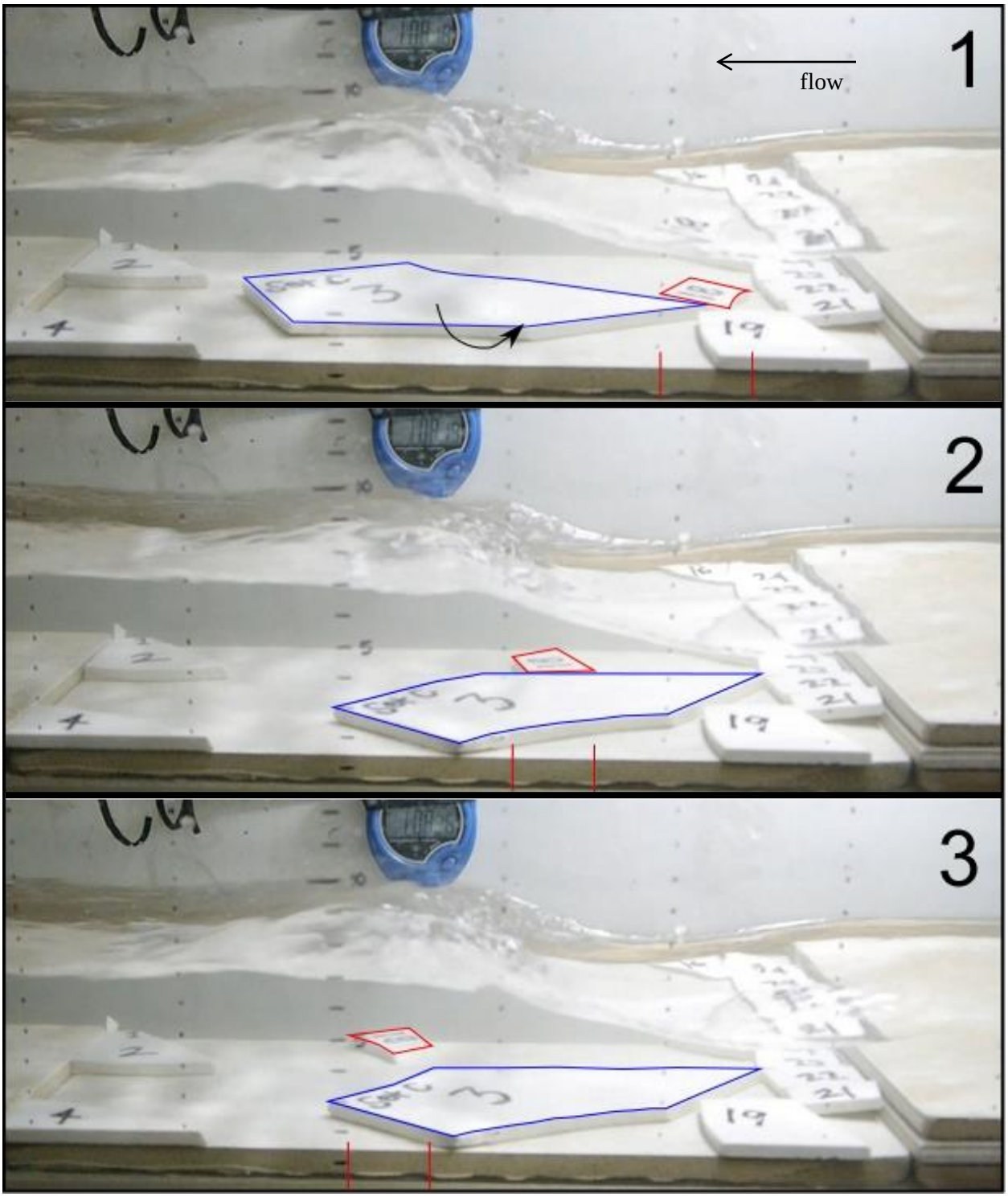

Figure 4. Lateral (blue) and downstream (red) sliding in the presence of a hydraulic jump. Sliding is the most common form of plucking when there is free space to move around the bed.

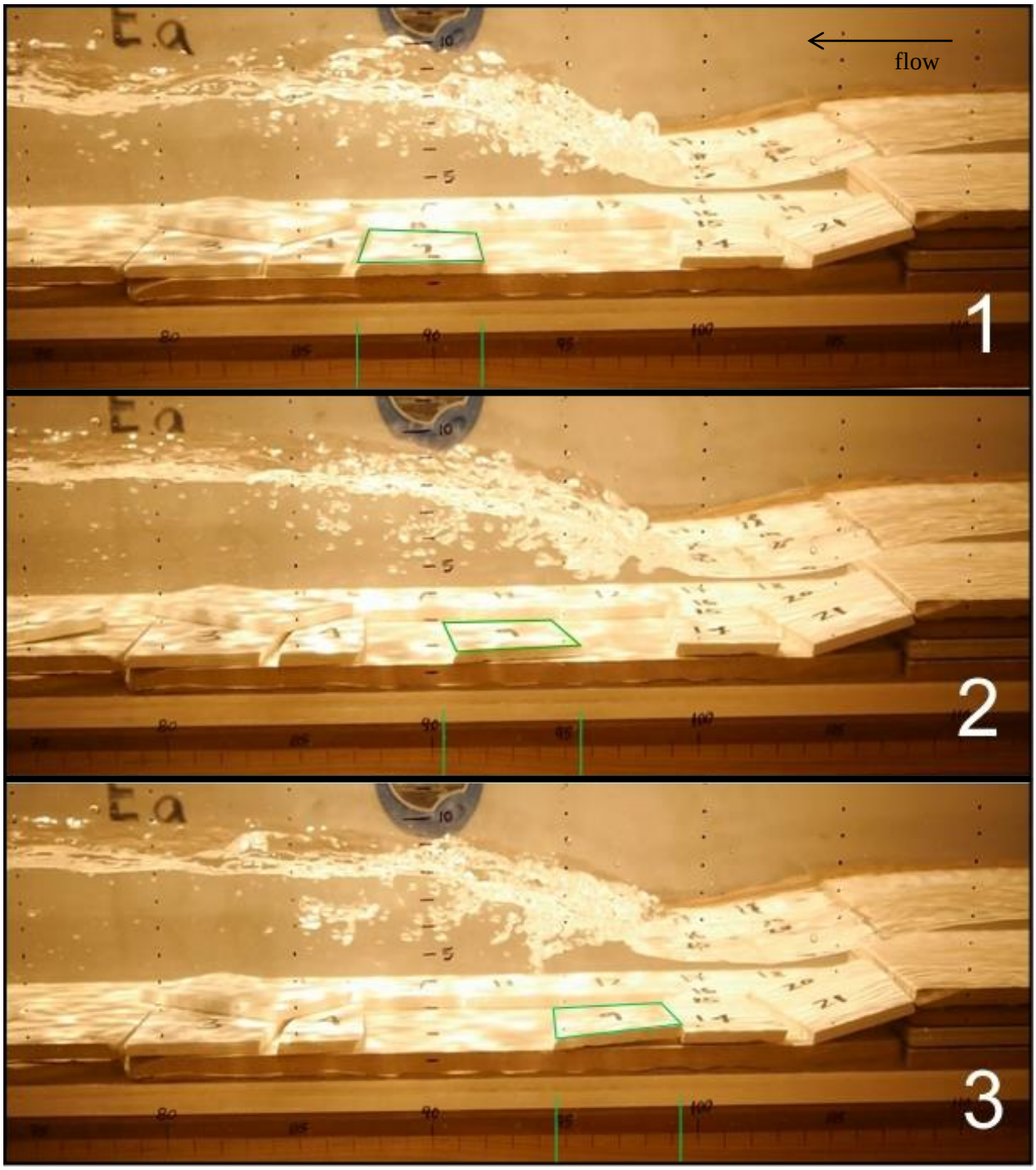

Figure 5. Upstream sliding of block 9 from an area of higher pressure to an area of lower pressure.

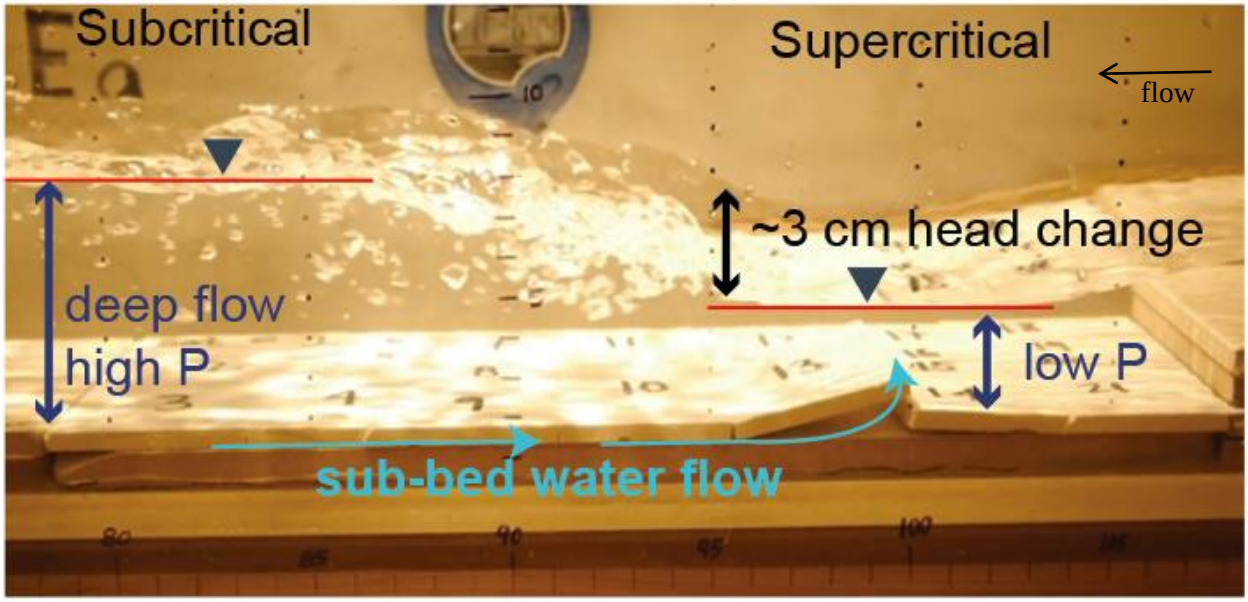

Figure 6. Hydraulic jump generated downstream of a modeled bedrock step. Adapted from (Harbor et al., 2015).

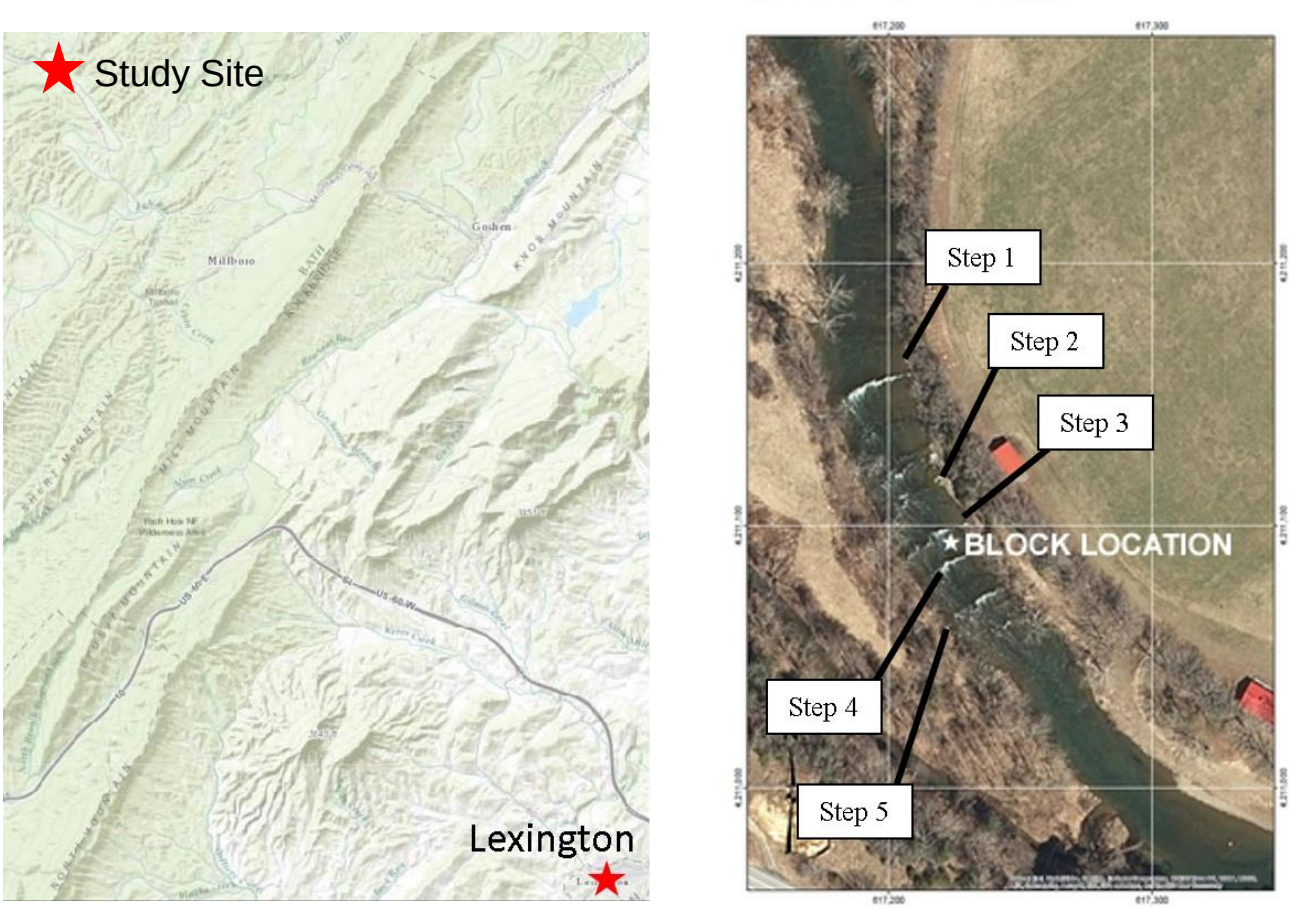

Figure 7. Study site, located in Bath County, VA. Block location is downstream of step 3, upstream of step 4.

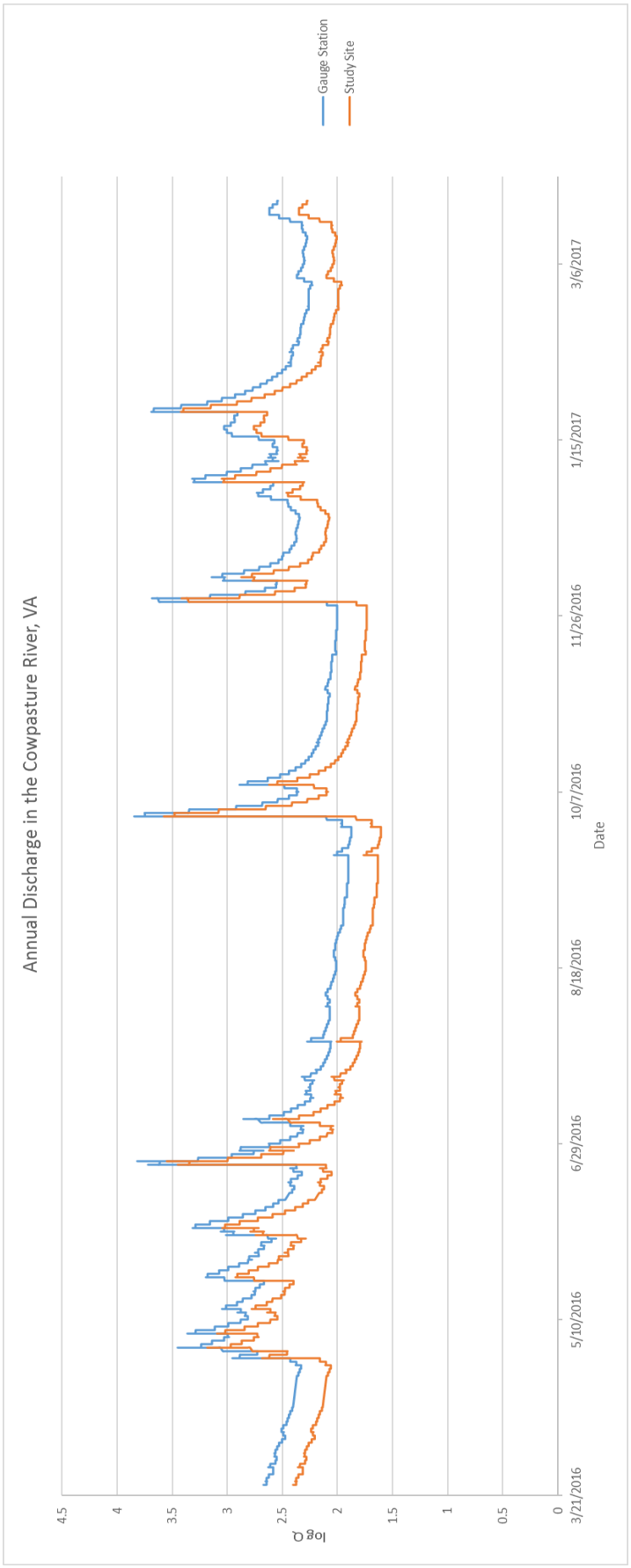

Figure 8. Discharge for the Cowpasture River at the gauge in Clifton Forge, VA (blue) and at the study site (orange), using the scaling ratio determined by Elium (2015). Gauge data from USGS Gauge 02016000.

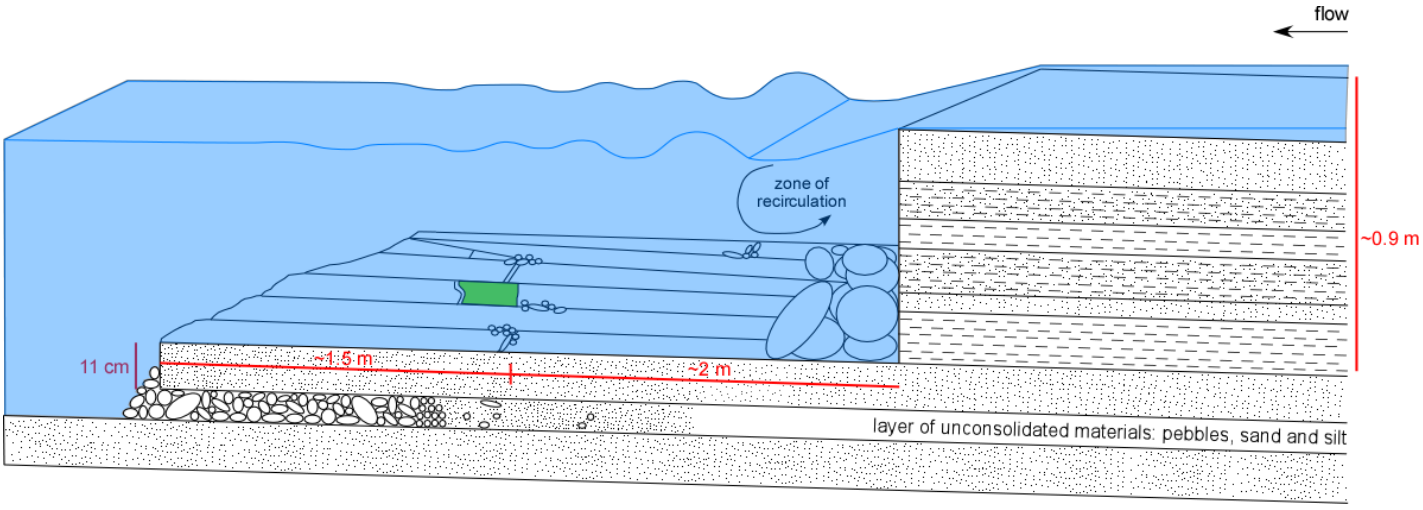

Figure 9. Schematic of study site, showing approximate block location (block highlighted in green). Hydraulic jump and chain of standing waves exist behind step 3 event in low-flow conditions.

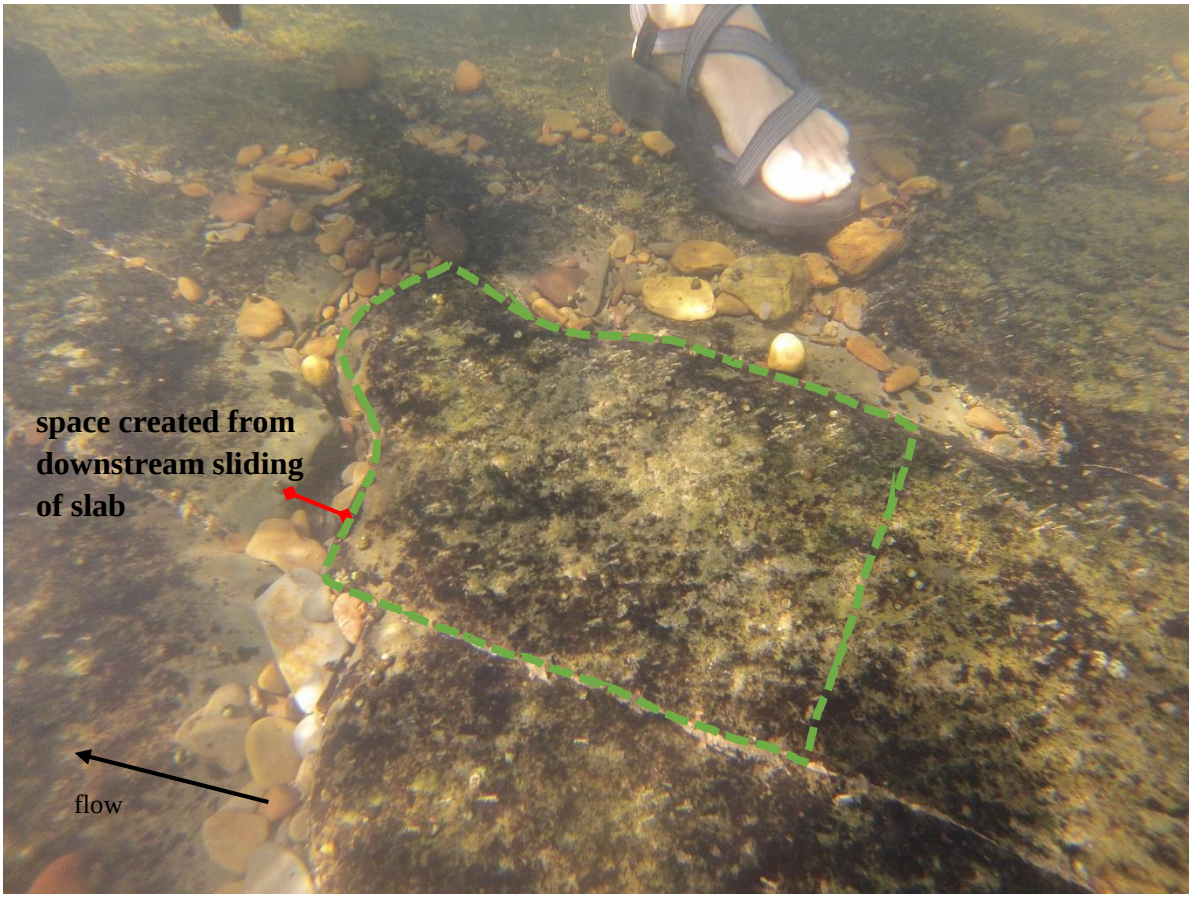

Figure 10. Evidence of downstream sliding. Notice accumulation of sediment in the enlarged cracks. This is also the selected study block before excavation (outlined in green).

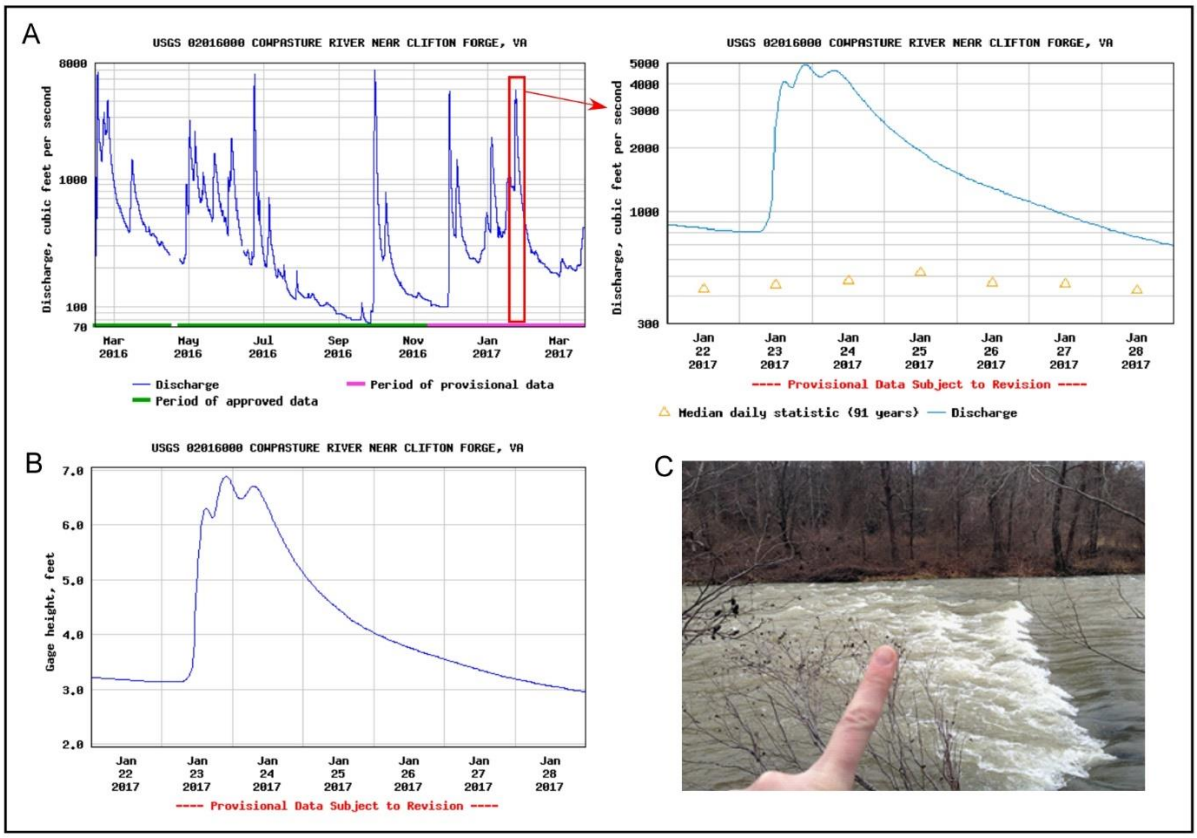

Figure 11. Water data from the USGS National Water Information System, recorded at station USGS 0201600, Cowpasture River near Clifton Forge, VA. A) Hydrograph recording 400 days of discharge; extent is the hydrograph for the Jan. 23 storm event. B) Gauge height during the Jan. 23 event. C) Image of Step 3 and the approximate location of the study block location during the Jan. 23 event.

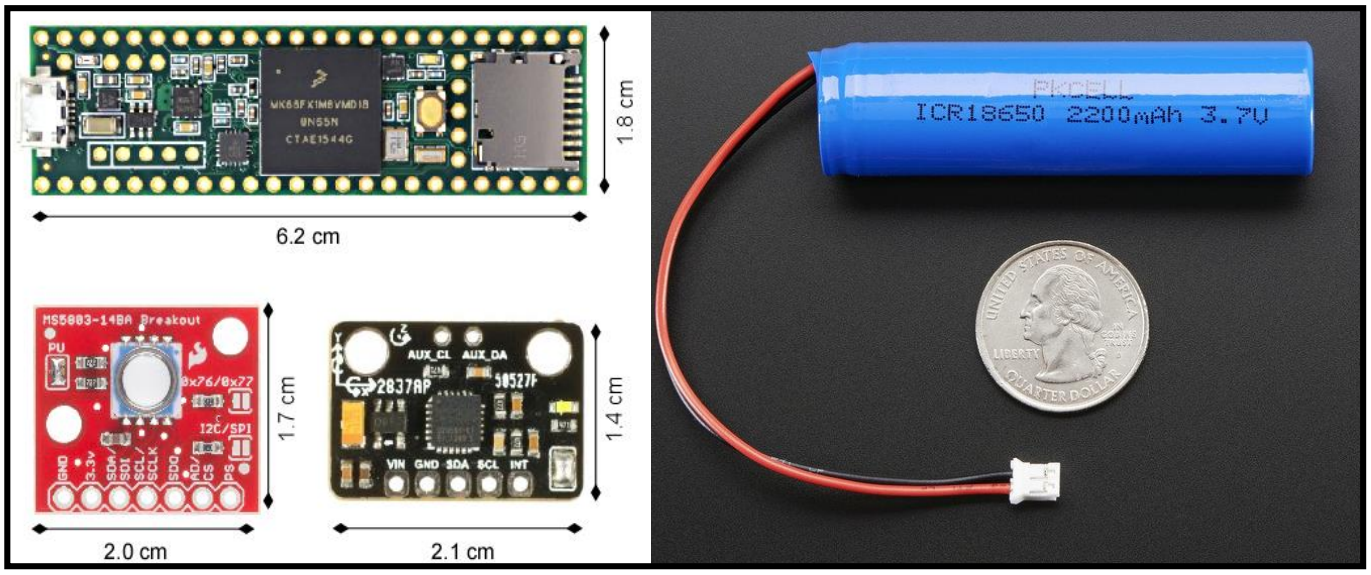

Figure 12. Electronics—green Teensy, red pressure sensor, black IMU and battery (stock images from websites).

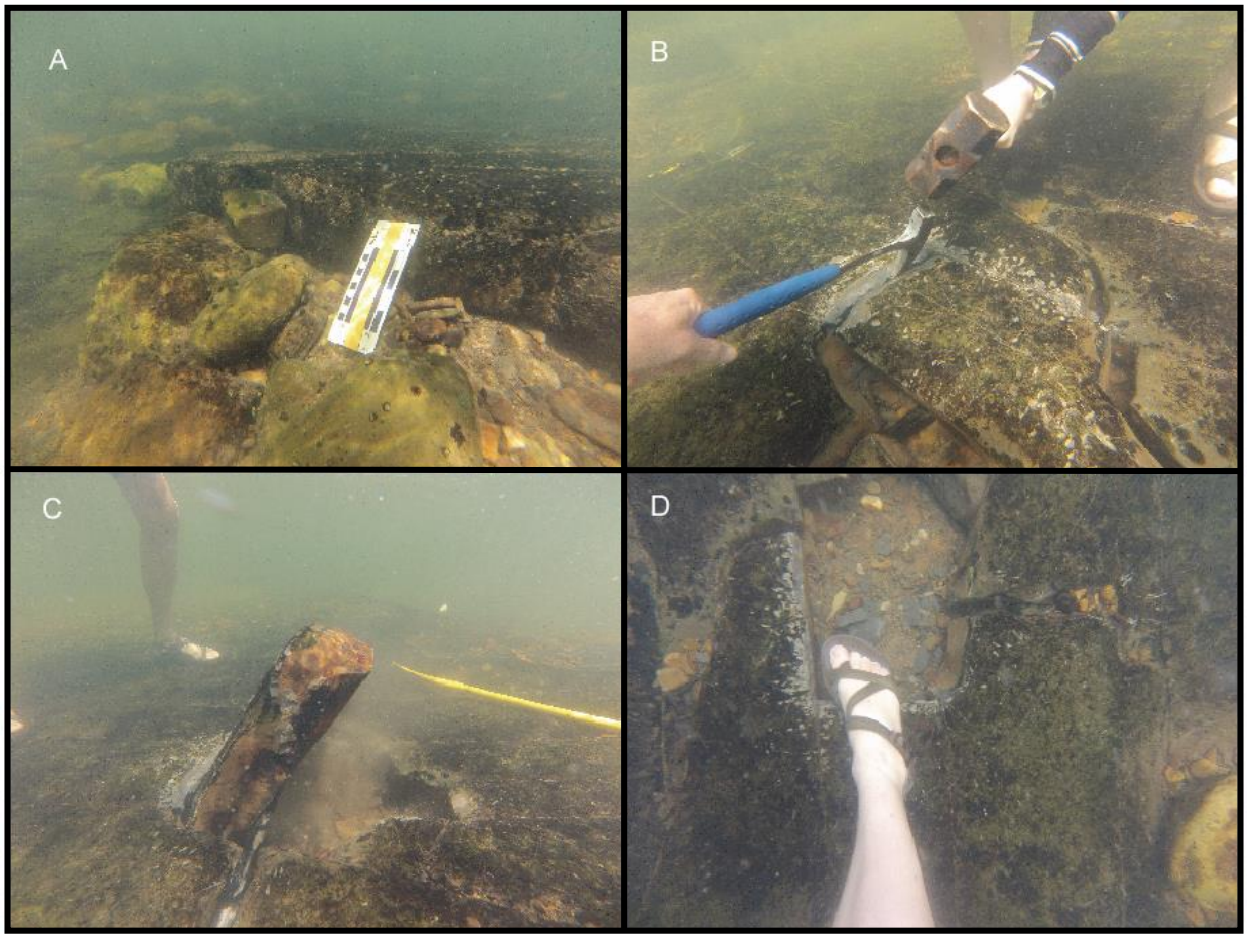

Figure 13. July 21, 2017 block extraction. A) Downstream lip of bed showing sediment accumulation and fractures. B) Hitting rock hammer with sledge to propagate energy radially. C) Lifting block out of bed using tamping bar. D) Sediment below extracted block, hole to which the block returns for river experiments.

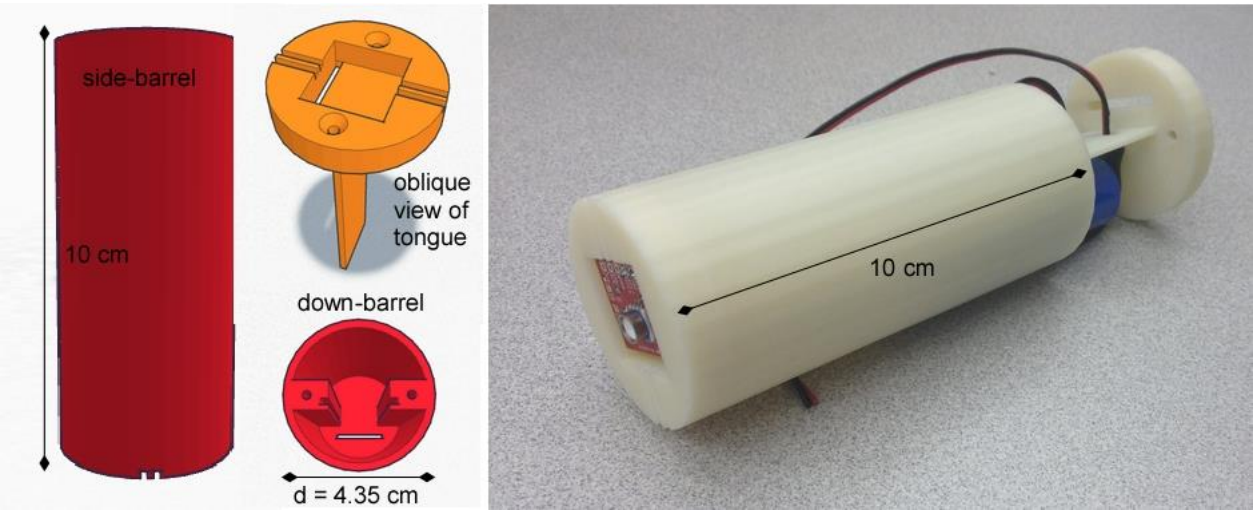

Figure 14. Capsule schematic.

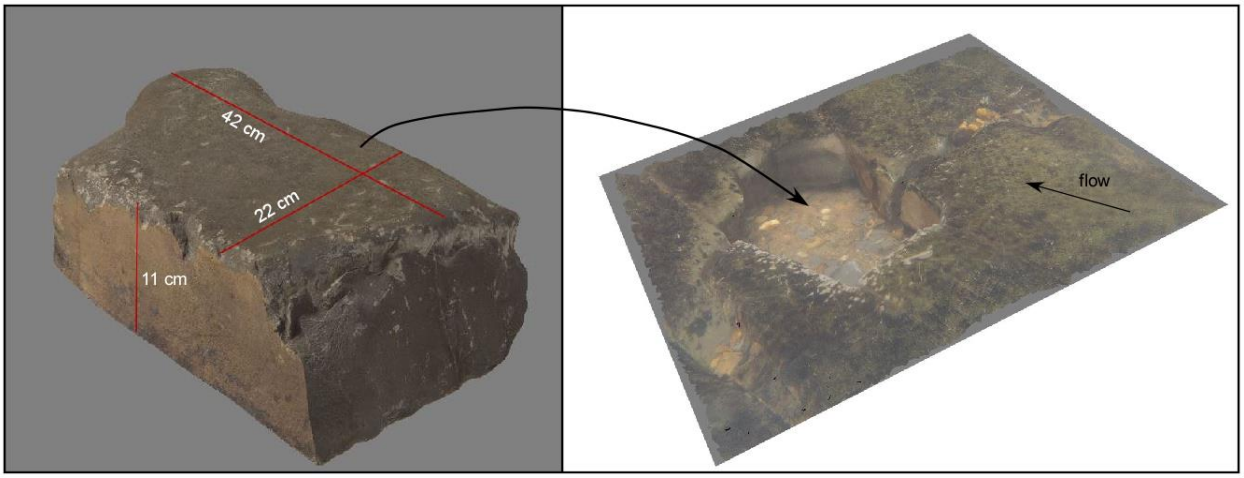

Figure 15. 3D model of block and excavation site, oriented to flow. Produced in Agisoft Photoscan.

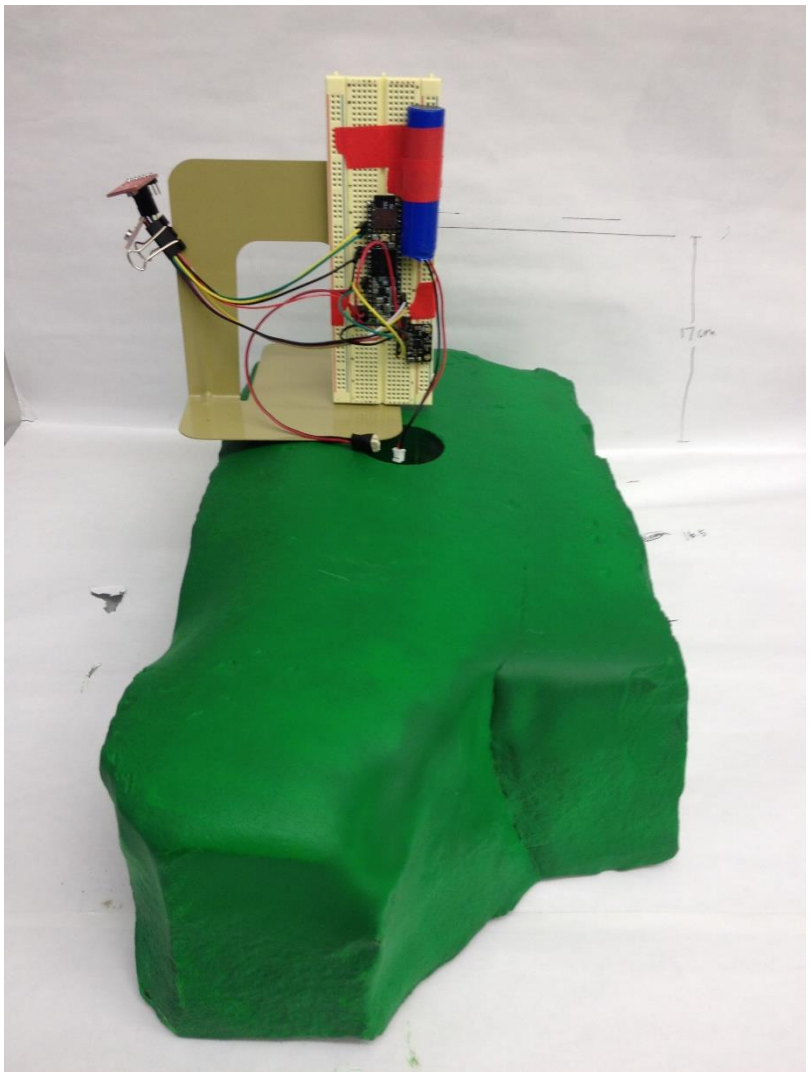

Figure 16. Breadboard setup with approximate orientation of electronics to block.

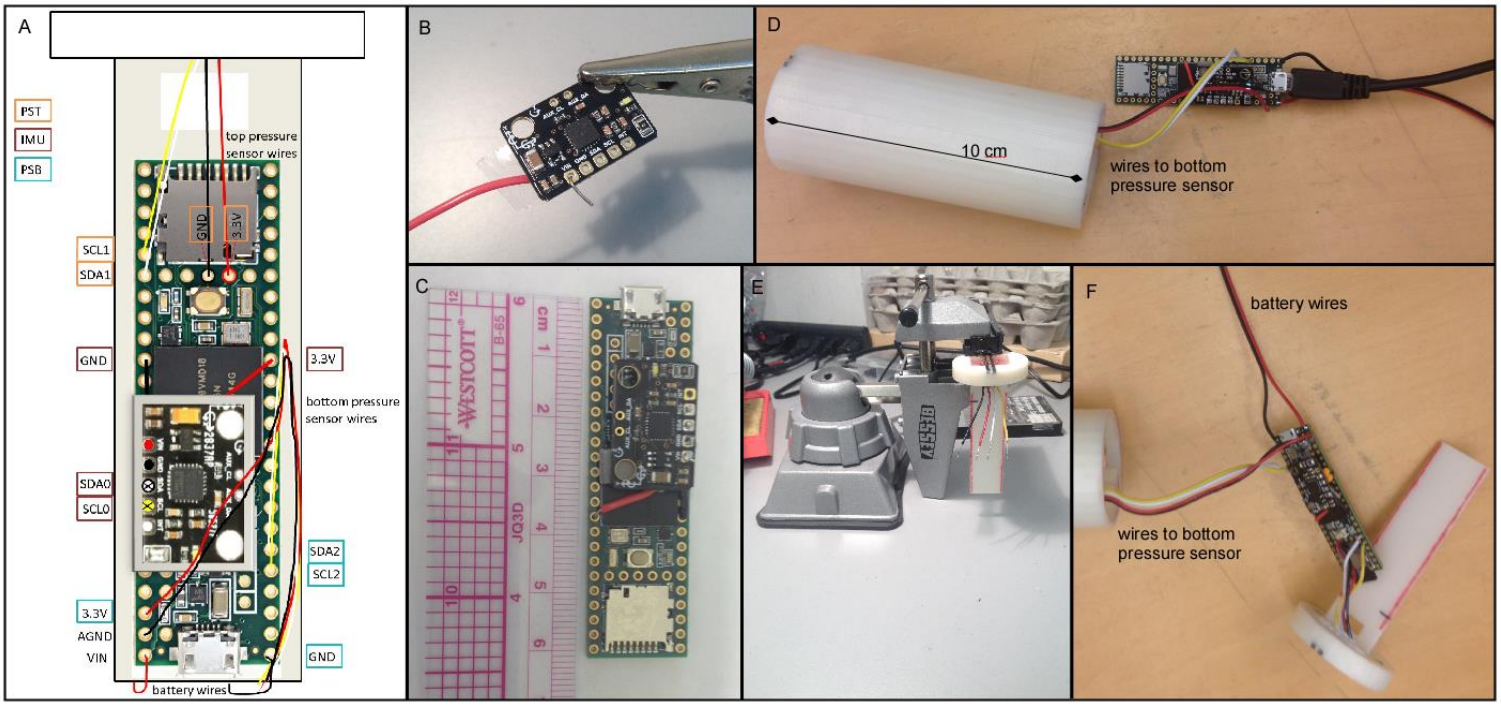

Figure 17. Electronics through various stages of assembly. A) Pinout showing approximate layout of wires. B) MPU6050 with hooked wire, not yet soldered. C) MPU6050 mounted on and soldered to Teensy. D) Bottom pressure sensor wires soldered to Teensy. E) Top pressure sensor with clipped wires. F) Teensy with soldered wires from all sensors.

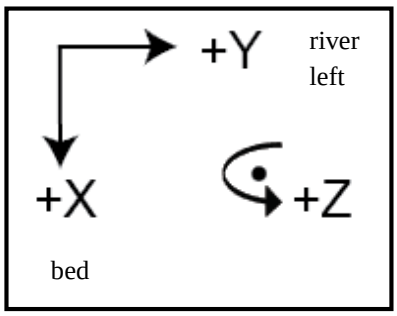

Figure 18. Axes orientation for MPU6050 when mounted in the capsule. This is the orientation the device takes when inserted in the rock. Flow is out of page along z-axis.

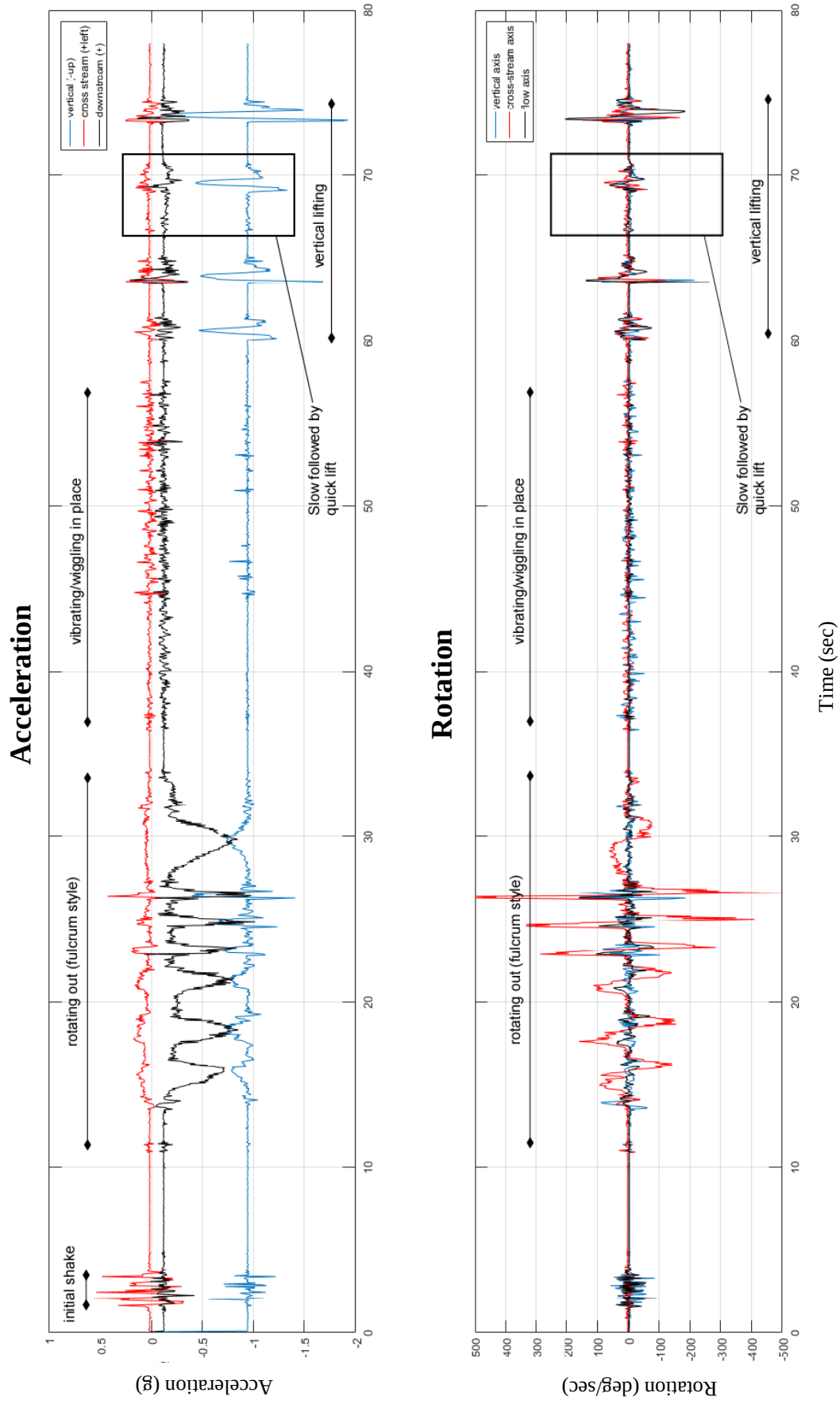

Figure 19. Breadboard experiment results.

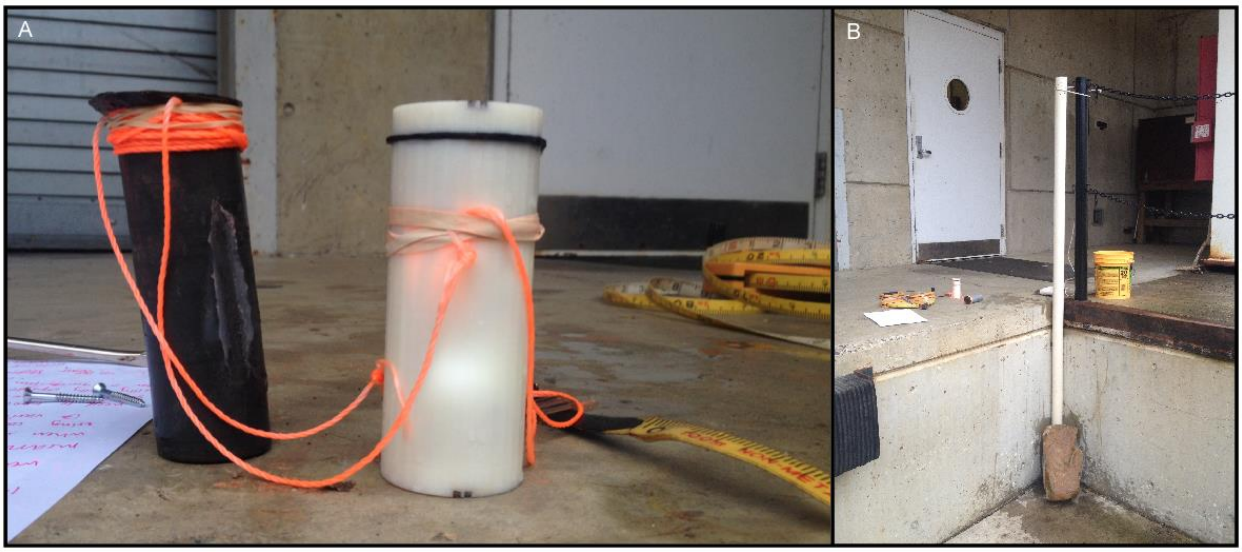

Figure 20. Still-water test setup. A) Sealed capsule attached to measuring tape and weight. B) PVC pipe secured in vertical position.

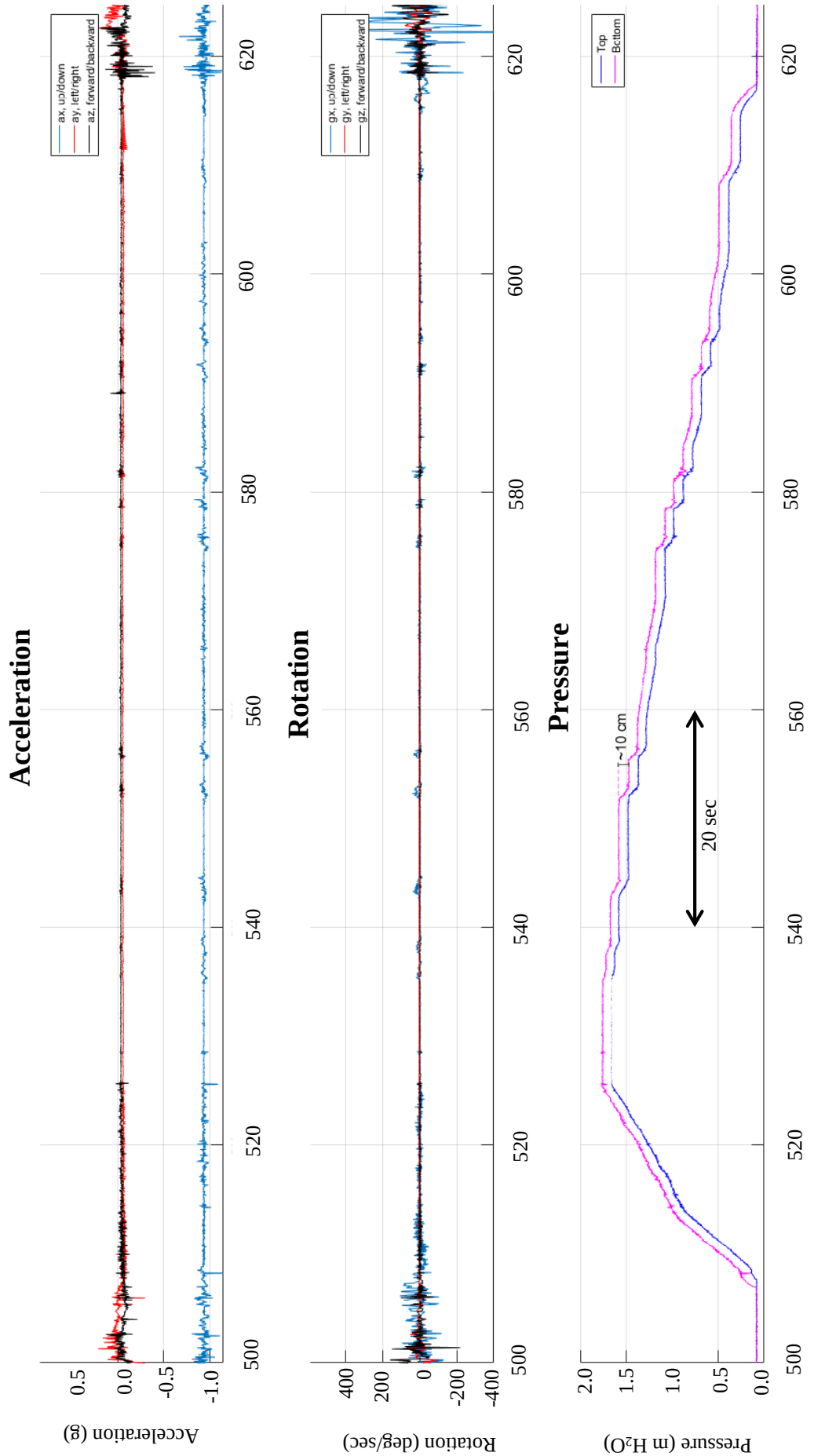

Figure 21. Still-water experiment results showing minimal acceleration and rotation in horizontal directions. Acceleration in the vertical direction and rotation around the vertical axis corresponds to each lift of the capsule. Pressure data shows a ~0.1 m decrease with each lift.

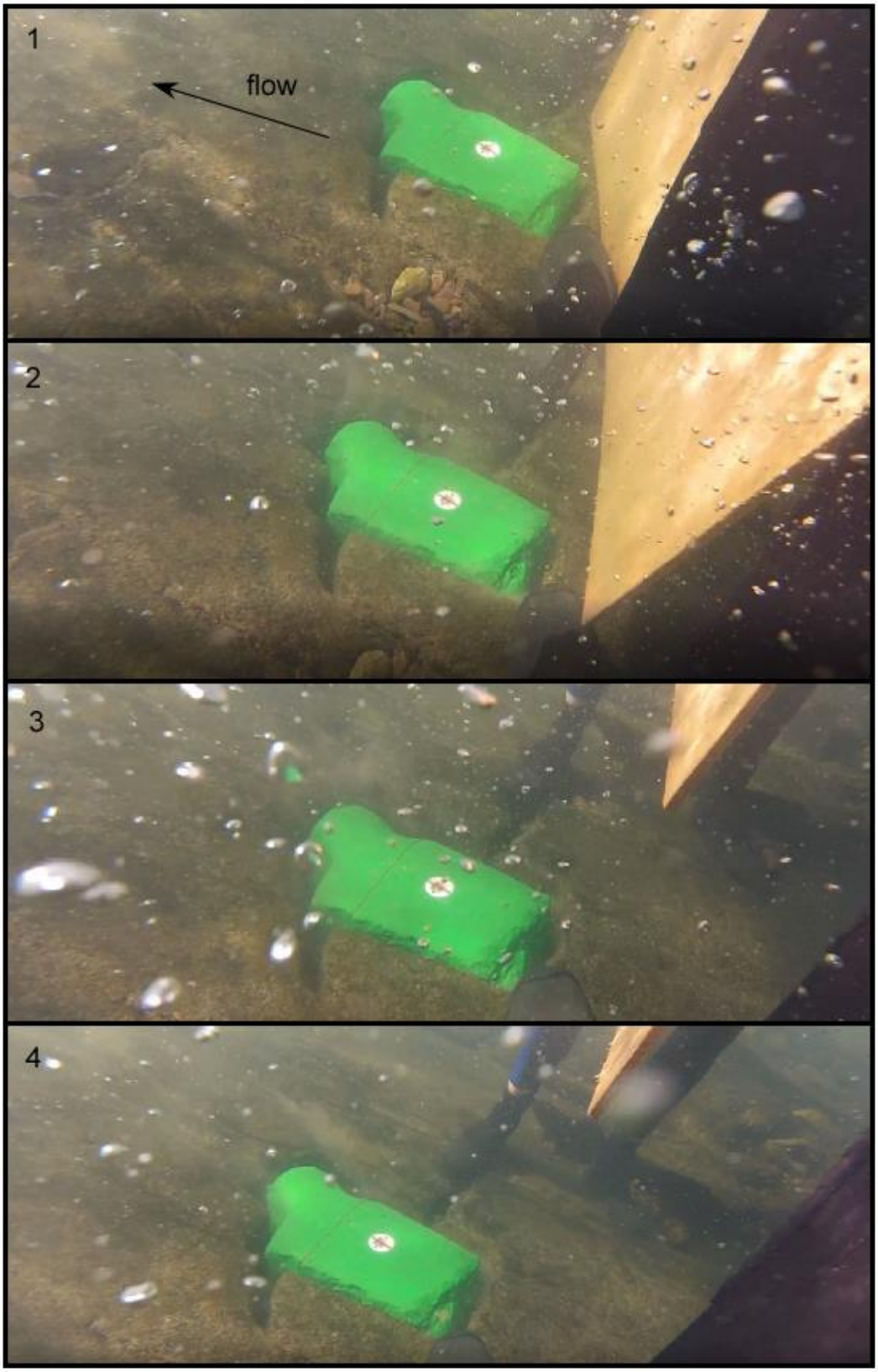

Figure 22. River test. Frames 1-4 show succession of lifting board vertically and introducing turbulence to the flow, indicated by increased presence of bubbles.

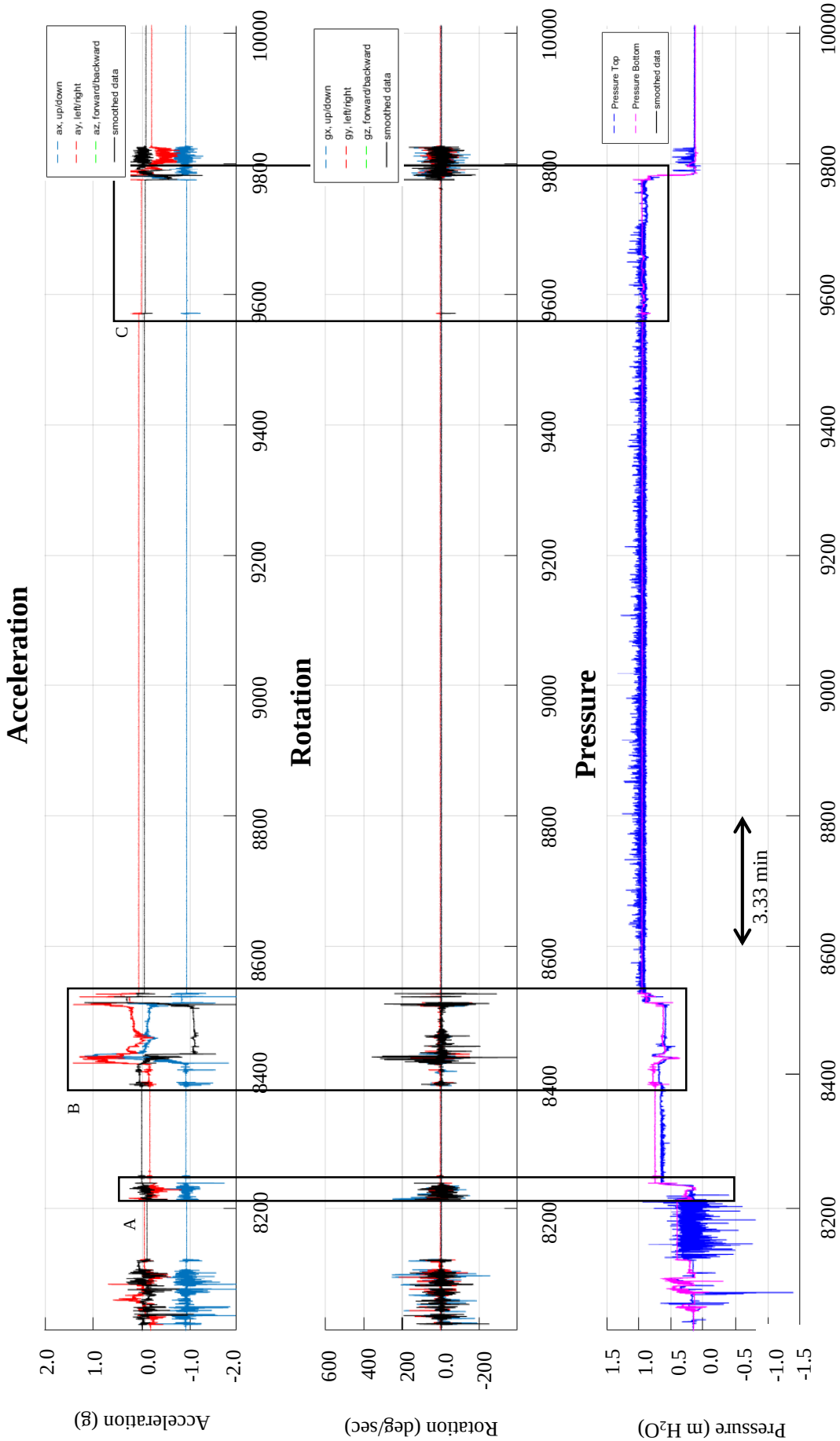

Figure 23. Wet test data. A) Dragging rock from bank to hole. B) Removing rock from crate and placing in hole. C) Board experiments—see Fig. 24 for detail

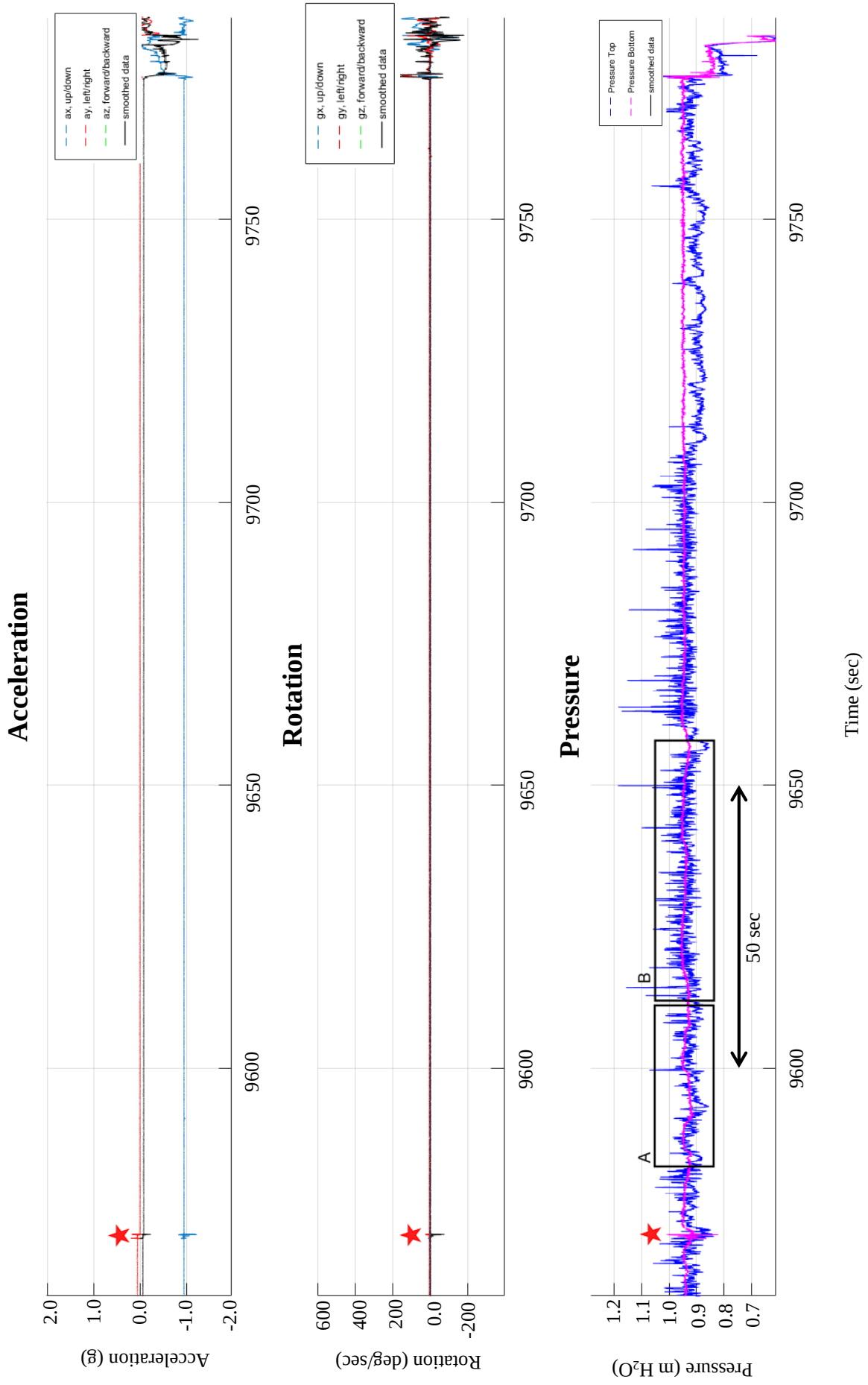

Figure 24. Detail of board experiments during river test. A) Short-wavelength oscillations in pressure readings while lifting the board close to the block. B) Longer-wavelength oscillations in pressure readings while lifting the board farther upstream. Red star indicates the board hitting the block.

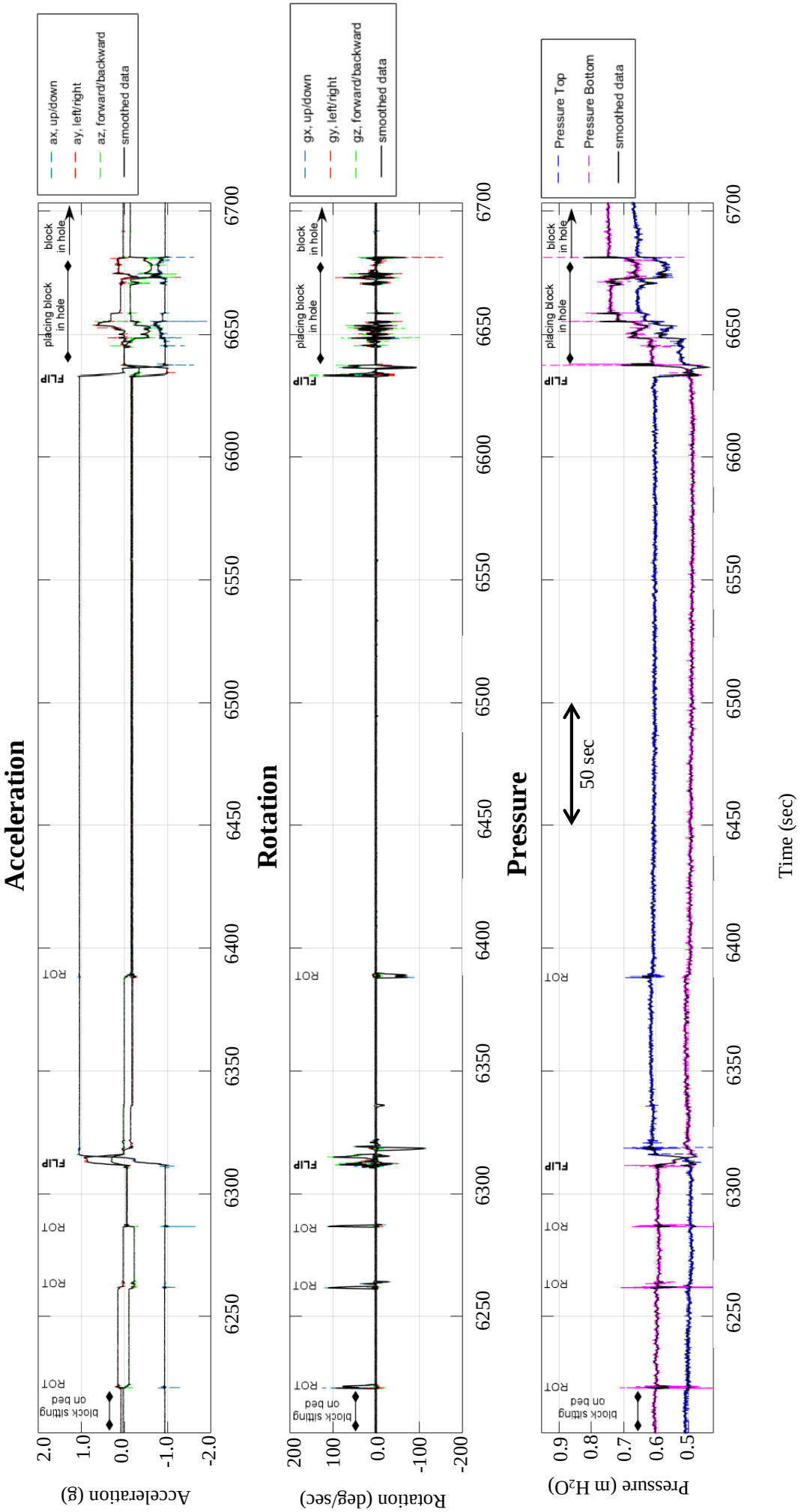

Figure 25. Detail of data from 24-hour experiment showing block rotations and flips.

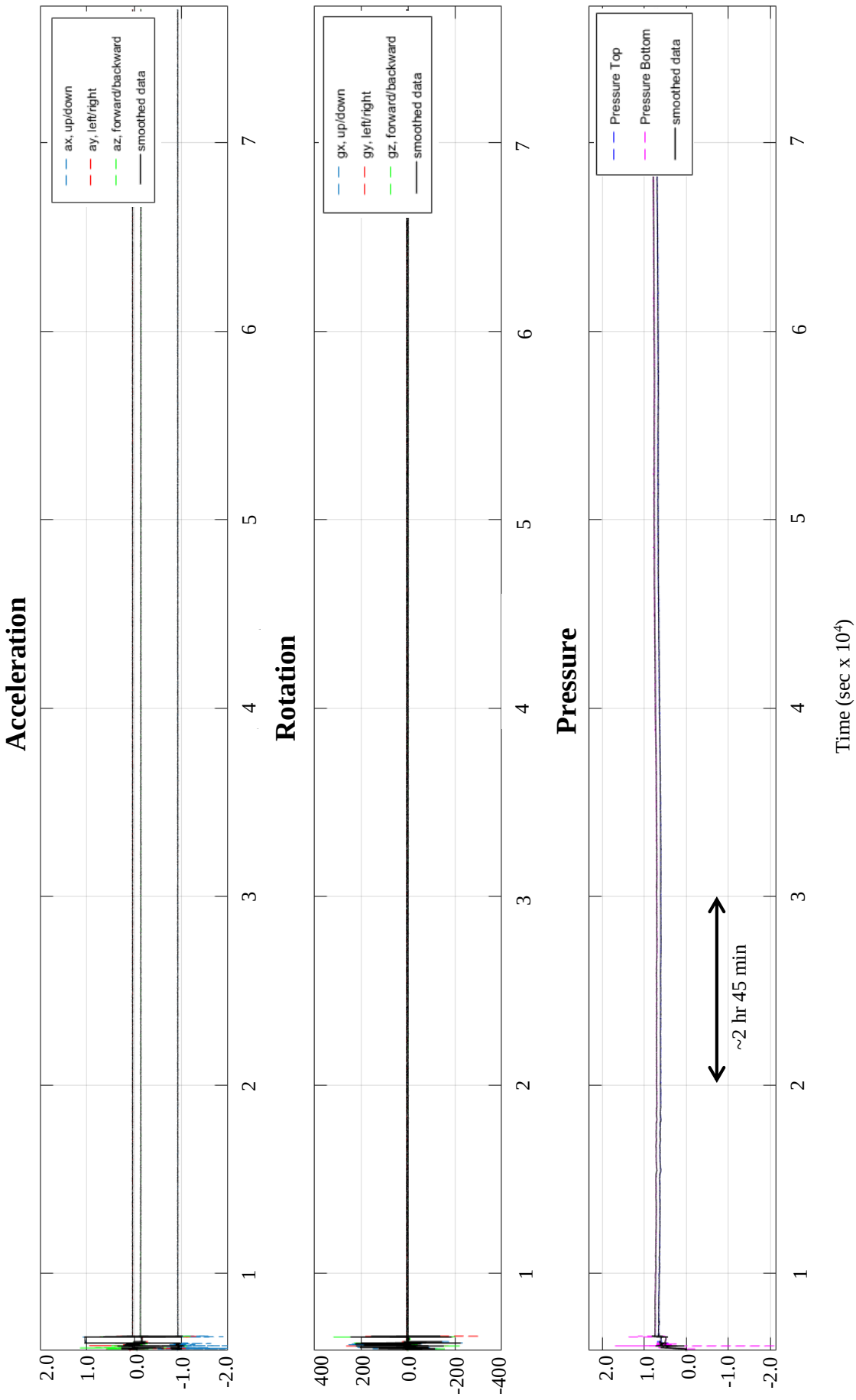

Figure 26. Full duration of 24-hour test. Block went into the river at approximately 2pm when discharge at gauge was 174 cfs and stage height was 1.82 ft. Recorded data until approximately 9am on March 2, when the gauge discharge was 214 cfs and stage height was 1.95 ft.

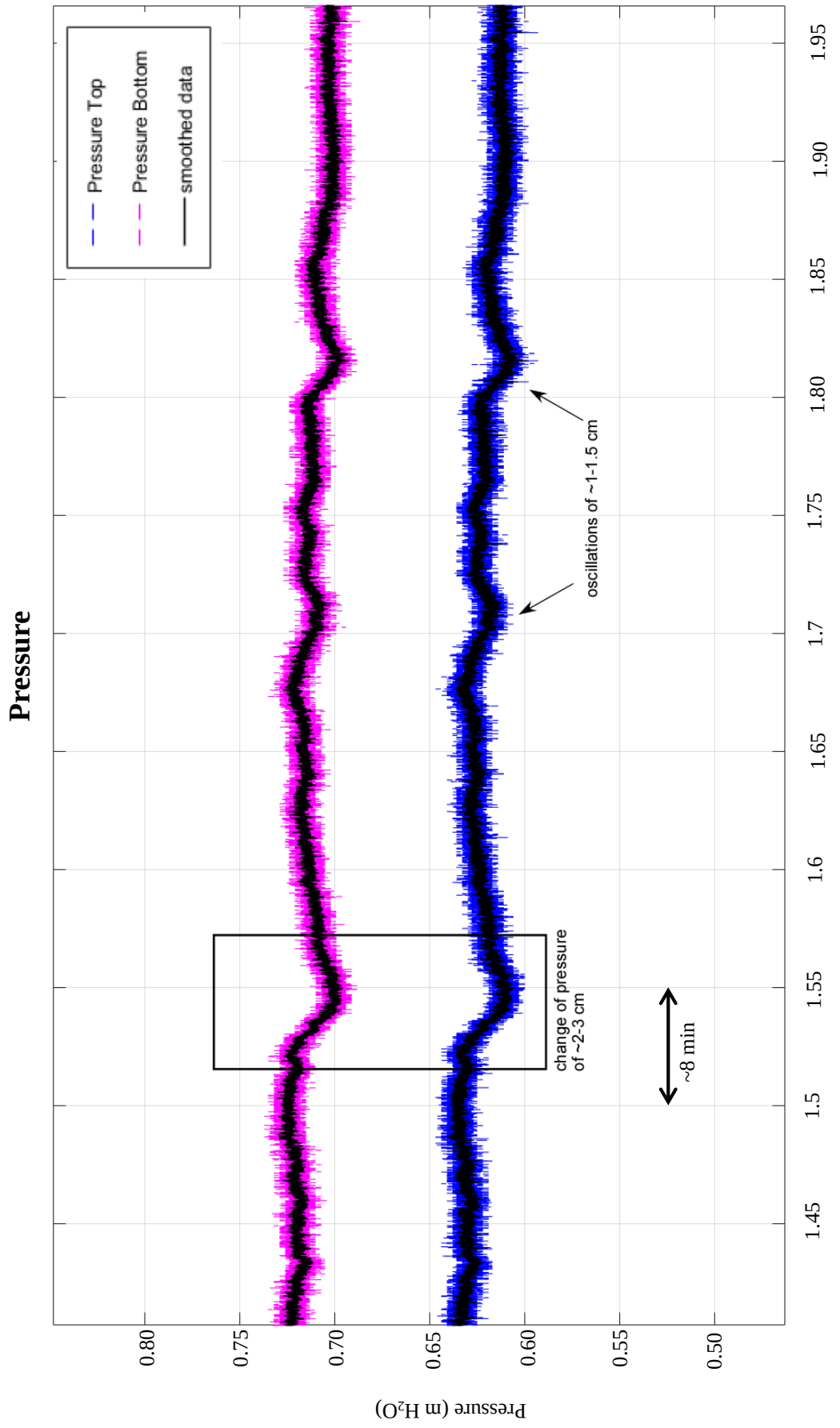

Figure 27. Pressure fluctuations that occurred roughly four hours after starting the device. Boxed section shows a change of ~2-3 cm of pressure over ~8 minutes.

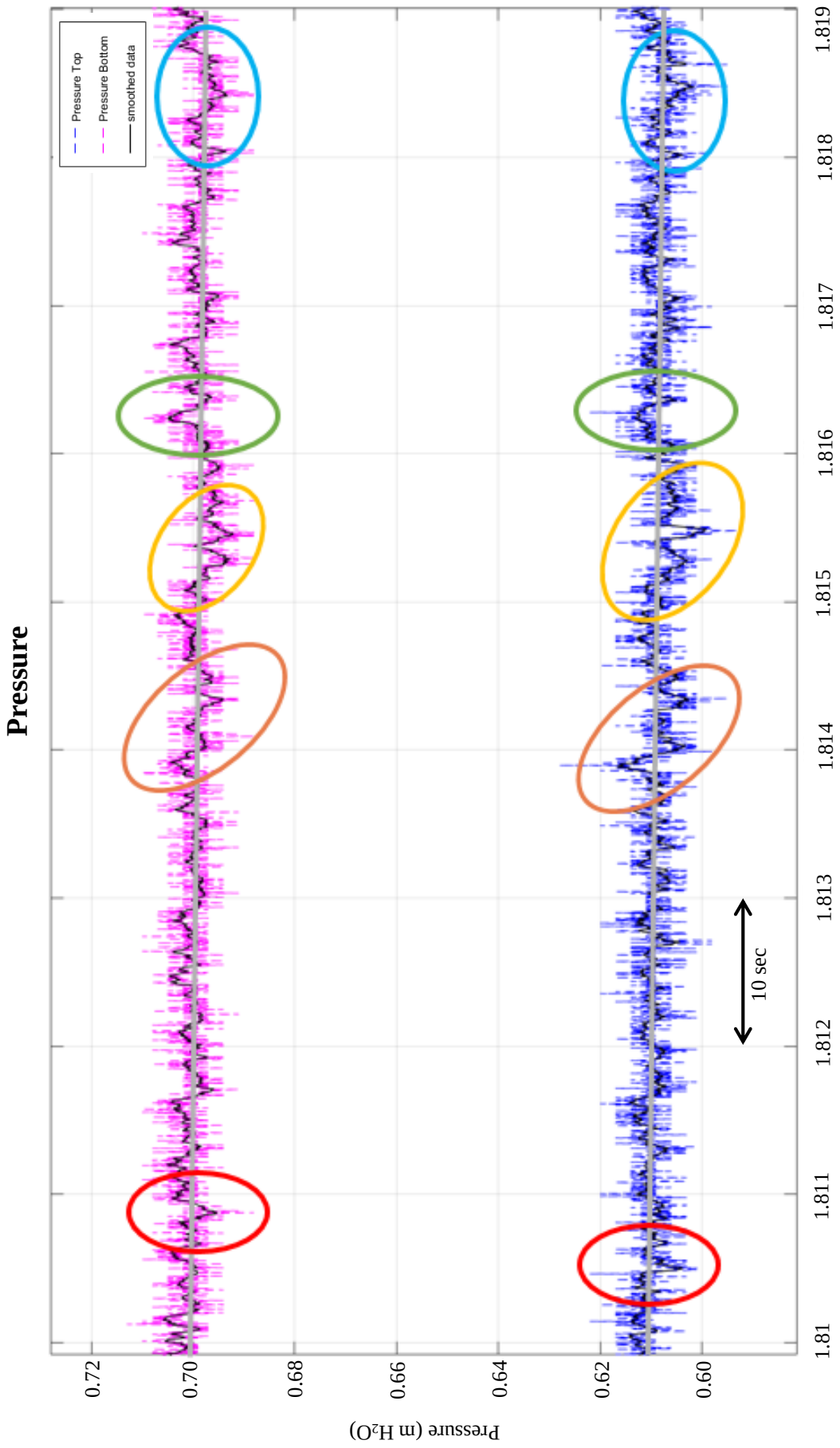

Figure 28. Detailed record of pressure fluctuations during the 24-hour experiment. Like-colored circles represent pressure changes that are possibly related.

A1: Variables used in force/lift calculations

Variable	Value
volume of block (m^3)	0.009353
mass (kg)	16.665175
Normal force (N)	163.485370
Pressure Pa	1993.724033
m of head	0.203233

S1: Supplemental Videos

Washington and Lee University file location: Q:\Research\plucking\Clare\Thesis Drafts\S1_Video
Online location: https://wlu.app.box.com/folder/23371936728

Description of videos:

Video 1: Breadboard test
Video 2: Board experiments during river test
Video 3: Block placement during 24-hour experiment, tests with dye in plastic baggie